

A Review of Dielectric Elastomer Generator Systems

Giacomo Moretti, Samuel Rosset, Rocco Vertechy, Iain Anderson, and Marco Fontana*

Dielectric elastomer generator systems (DEGSs) are a class of electrostatic soft-transducers capable of converting oscillating mechanical power from different sources into usable electricity. Over the past years, a diversity of DEGSs has been conceived, integrated, and tested featuring diverse topologies and implementation characteristics tailored on different applications. Herein, the recent advances on DEGSs are reviewed and illustrated in terms of design of hardware architectures, power electronics, and control, with reference to the different application targets, including large-scale systems such as ocean wave energy converters, and small-scale systems such as human motion or ambient vibration energy harvesters. Finally, challenges and perspectives for the advancement of DEGSs are identified and discussed.

or distributed sensing/monitoring systems.^[1–5] On the other hand and on the large scale, there is a growing demand of grid electricity which should be produced starting from novel sustainable/renewable energy resources.^[6–9]

These new requirements have pushed researchers to conceive solutions to scavenge forms of mechanical energy in conditions where conventional electromechanical generators struggle to excel. In particular, novel energy conversion devices have been conceived with the aim of improving electricity generation from non-steady sources of power that are associated with oscillating/time-varying forces and motions. These include the vibration of

structures, relative motion between machine components, human motion, and natural sources of energy such as waves or wind.

Toward this aim, several novel mechanical-to-electrical energy conversion principles have been studied and demonstrated in the form of generators based on linear electromagnetic devices,^[10] triboelectric materials,^[11] pyroelectric,^[12] reverse electrowetting,^[13] carbon nanotube yarns,^[14] and dielectric elastomers (DEs).^[15]

Among them, the class of DE generators (DEGs) represents a promising alternative. DE transducers were conceived at the end of past century. By leveraging on an electrostatic variable-capacitance principle, they can pursue different operation modes, such as actuators, generators, and sensors.^[16,17] Their operation relies on the variable electrostatic capacitor principle. Specifically, DEGs are considered as a very promising energy conversion technology thanks to their attributes of: 1) intrinsically cyclical working principle that well matches alternating/time-varying quality of the mechanical energy; 2) high energy densities of up to theoretical values of 3 J g^{-1} ^[18] and experimental values of up to 0.78 J g^{-1} ;^[19] 3) convertible energy density which is theoretically independent of the operating frequency; 4) low-cost of the raw materials; 5) light weight, architectural simplicity (with few or no moving rigid parts), and silent operation. In contrast with piezoelectric or electromagnetic generators, which struggle to adapt to millimeter- or meter-scale, respectively,^[20–22] the layout and principle of DEGs can be virtually adapted to different dimensional ranges, enabling a diversity of applications, from human motion to renewable energy harvesting.^[23]

To accomplish the generation task, DEGs are equipped with driving electronics, capable of controlling their electrical activation, and a sensing system, that makes it possible to evaluate the state of the DEG and to manage the electrical activation accordingly. The combination of DEG, conversion electronics, and sensing system is here referred to as the dielectric elastomer generator system (DEGS).

1. Introduction


The technology used to achieve the conversion of available mechanical energy into usable electricity has been vastly dominated by electromagnetic systems based on Lorentz force or variable inductance. However, in the past decades, the demand and the type of use of electrical power has gone through significant changes, bringing new needs and challenges. On the one hand, there is a need of electricity sources in the small-scale range to provide or extend the power supply for emerging devices such as wireless, portable, wearable, implantable electronics,

Dr. G. Moretti
TeCIP Institute
Scuola Superiore Sant'Anna
Pisa, Italy

Dr. S. Rosset, Prof. I. Anderson
Bioengineering Institute
University of Auckland
Auckland, New Zealand

Prof. R. Vertechy
Department of Industrial Engineering
University of Bologna
Bologna, Italy

Prof. M. Fontana
Department of Industrial Engineering
University of Trento
Trento, Italy
E-mail: marco.fontana-2@unitn.it, marco.fontana@santannapisa.it

 The ORCID identification number(s) for the author(s) of this article can be found under <https://doi.org/10.1002/aisy.202000125>.

© 2020 The Authors. Published by Wiley-VCH GmbH. This is an open access article under the terms of the Creative Commons Attribution License, which permits use, distribution and reproduction in any medium, provided the original work is properly cited.

DOI: 10.1002/aisy.202000125

This article aims at reviewing the current state of the DEGS including aspects related to the choice of topology, electronics, and control. In addition, DEGS are analyzed in the context of their application including the harvesting of energy from human motion power, structural and machine vibrations, and renewable energy sources. The article is organized as follows. In Section 2, generalities and working principle of DEG are presented, including a summary of the available generator topologies that have been conceived and implemented so far. Section 3 is focused on the different types of driving and control electronics that are used for laboratory prototypes, distributed and wearable applications, and large-scale energy harvesting. Section 4 presents a critical overview of the different applications for which DEGS have been devised and studied. Section 5 presents the conclusions and a discussion on open challenges and future research and development directions.

2. Generalities on DEGS

2.1. Operating Principle

A DE transducer consists of a layer of deformable elastomeric dielectric material (namely, the DE), coated with compliant electrodes so as to form a variable capacitor.^[17] In general, a DE transducer can work either as an actuator, a generator, or a sensor. In the actuator mode, electrostatic forces are used to induce the capacitor's deformation and make work against a mechanical load.^[16] In generators (DEGs), the capacitor is cyclically deformed by external mechanical forces, leading to an increase in the electrostatic potential energy of the charges present on the electrodes.^[24] Finally, in DE sensors, capacitance variation measurements are exploited to sense a stretch or an applied force.^[25]

Specifically, the operating principle of a DEG can be described in terms of a cyclic sequence of electromechanical transformations. To give an example, we make reference to a position-controlled planar DEG unit subject to uniform stretches on the electrodes plane, driven according to a cycle (Figure 1a) with the following phases:

(P1) As the DEG initially dwells in configuration (A), where its capacitance is minimum (C_{\min}), external loads make it expand

and lead it to configuration (B), where the capacitance is maximum (C_{\max}). During this phase no charge is present on the DEG.

(P2) As the DEG configuration is held locked, charge Q is deposited on the electrodes, leading the DEG to state (C) (where the capacitance is the same as in (B)). This phase is called "priming," and it involves an amount of electrical energy be spent to charge the device.

(P3) As the charge on the DEG is held constant, the external loads and/or the DE elastic stresses make work against the electrostatic charge, taking the DEG back to a configuration (D) with minimum capacitance, C_{\min} . During this generation phase, electrostatic energy is produced at the expense of the work supplied by the external forces, and it is stored in the DEG electric field.

(P4) The DEG is finally held in the minimum capacitance configuration and discharged, and the stored electrostatic energy is harvested.

The net amount of generated electrical energy is the difference between the energy recovered during the discharging phase (P4), and that spent during priming (P1). Such energy increases monotonically with the difference in capacitance between the stretched and the initial configurations (C_{\max} and C_{\min}) and with the maximum applied charge (or electric field).

The described sequence of electromechanical transformations can be graphically represented on a charge–voltage, Q – V , plane. In Figure 1b, the electrically active phases (P2–P4) of the operating cycle are represented by a sequence of curves rendering the working cycle. In particular, the priming phase (P2) is represented by isocapacitance straight line (C)–(B), the generation phase (P3) (here, a constant charge [CC] phase) corresponds to line (C)–(D), and the discharging phase (P4) is represented by isocapacitance straight line (D)–(A). The amount of energy spent during priming equals the area subtended by segment (B)–(C), whereas the energy recovered during DEG discharging equals the area subtended by (D)–(A). The area enclosed by the cycle hence equals the net generated electrical energy.

Though in the previous example, we referred to a piecewise CC control (i.e., the charge on the electrodes is held constant during phases (P1) and (P3)), different controls are possible, as further discussed in Section 2.4.

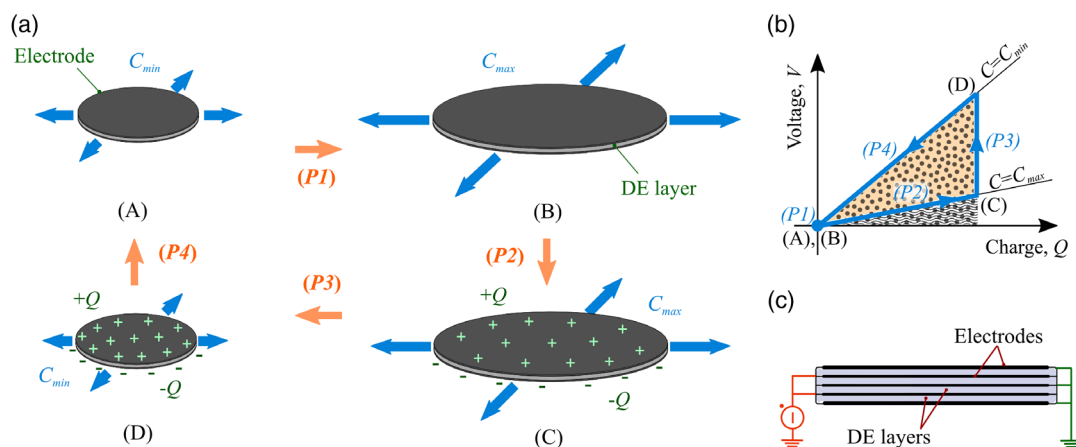


Figure 1. a) Four-phase working cycle of a DEG. b) Representation of the working cycle phases on a charge–voltage Q – V plot. (c) DEG stack layout.

Multiple units can be stacked up and electrically connected in parallel to form a DEG with the same surface encumbrance as the units, capable of converting a larger amount of energy.^[26] This results in a multilayer composite DEG structure, in which consecutive DE layers are separated by conductive layers with alternated polarity, as shown in Figure 1c. Arranging the DE material in a stack of separate layers, rather than a single thick layer with a couple of electrodes allows the implementation of large electric fields (and, hence, the achievement of large convertible energy density), at lower voltages on the electrodes.

2.2. Topologies

The operating principle described earlier can be implemented using different DEG embodiments, in the same fashion as DE actuators.^[27] Resorting to different DEG topologies provides a significant flexibility in application to practical systems. Nonetheless, different topologies provide different deformation kinematics for the DE membranes, which result in different performance.

An overview of some relevant DEG topologies is shown in Figure 2. The simplest DEG planar topologies (in which stretching is generated by loads applied at the electrodes perimeter) feature deformation kinematics that in continuum mechanics literature^[28–30] are referred to as equibiaxial (or equal-biaxial)^[31] stretching (Figure 2a), and pure-shear stretching (Figure 2b), also called strip-biaxial extension.

A so-called equibiaxial extension consists in a uniform stretching of a DE membrane along each direction on the electrodes plane; this maximizes the capacitance variation achieved in the presence of a given maximum material stretch.^[32] Coupling a DEG membrane with a practical system so as to achieve equibiaxial stretching is technically complex. For the aim of experimental demonstration, mechanisms providing nearly equibiaxial stretching have been built,^[33] using a set of pulling wires connected along the membrane perimeter (Figure 2a). Equibiaxial stretching has been alternatively achieved through the implementation of compression stacks, in which electrodes' surface expansion is generated by the application

of a compressive force perpendicular to the electrodes plane.^[26] This approach allows to arrange large volumes of DE material into self-supporting structures with no need for rigid frames. With reference to equibiaxial compressive stacks, Anderson et al. observed that the stack aspect ratio (diameter over height) influences the stretch distribution, as it might cause inhomogeneous stretching of the different layers, especially in the presence of large diameter-to-height ratios.^[34] Pure shear (or strip-biaxial) stretching, in contrast, consists in the application of a force at the clamped end of a DEG strip, whose transversal stretch is held constant, so as to cause an expansion in the longitudinal direction (Figure 2b).^[35] A uniform transversal prestretch is applied to prevent loss of tension. In contrast with the longitudinal stretch, no stretch variation takes place in the transverse direction during operation. The pure-shear kinematics leads to limited capacitance variations on the DE membranes, but offers good ease of implementation. In practice, keeping the transverse prestretch uniform upon longitudinal stretching, thus preventing necking of the free membrane sides, is challenging. Lateral shrinkage can be mitigated by using slender samples with large transverse breadth compared with the length, or by using mobile lateral clamping mechanisms.^[35] Both these solutions, however, significantly limit the applicability onto real-world systems. Reducing the membrane width and increasing the sample longitudinal initial length would lead to a uniaxial topology (also known as simple elongation^[36]). Compared with pure shear, uniaxial deformation would produce further limited capacitance variations upon longitudinal stretching, therefore its usage in DEGs is considered of scarce practical interest.^[37]

To overcome the practical limitations of equibiaxial and pure-shear DEGs, planar DEGs can be implemented by connecting the perimeter of a DE membrane to a closed-chain linkage. The diamond DEG (or parallelogram DEG) shown in Figure 2c,^[38,39] e.g., is a practical topology that consists in a rhombus-shaped DEG membrane clamped through its perimeter to the links of a four-bar mechanism with four equal links. The membrane is biaxially preloaded along the diagonals, and its surface (together with the DEG capacitance) is maximum when the

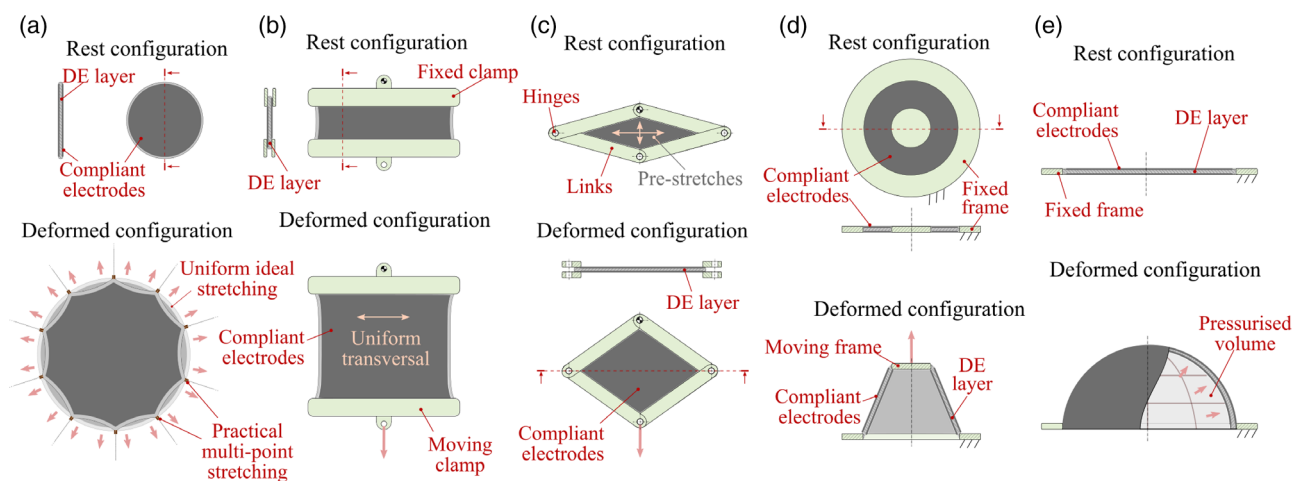


Figure 2. Some topologies of DEG. a) Equibiaxial DEG (ideal uniformly stretched generator, and practical multipoint stretching embodiment); b) pure shear (namely, strip-biaxial) DEG; c) diamond DEG; d) cone DEG; and e) circular diaphragm DEG.

relative angles between adjacent links are 90° (i.e., when the membrane has square shape). This device can work both as a linear generator (dragged by an external force) or a rotary generator (driven by a pulsating torque). As a linear generator, the DEG is linearly stretched along the diagonal direction through a couple of opposite joints (as shown in Figure 2c). As a rotary generator, the DEG exploits the rotation between two adjacent links.^[39] Due to the mechanism kinematics, an increase in stretch in a diagonal direction corresponds to a relaxation of the stretch in the perpendicular direction. In this topology, the achievable area strain is thus limited compared to the pure-shear or equibiaxial kinematics.

Other practical DEG topologies take advantage of out-of-plane deformations of DE membranes. Among them, the conical DEG (Figure 2d)^[40–42] consists in a uniformly prestretched annular DEG membrane, clamped on the external perimeter to a fixed ring frame, and on the inner perimeter to a mobile rigid disc. Applying longitudinal forces on the rigid disc deforms the DEG to a conical configuration. The cone DEG capacitance is minimum when the DE membrane is in the flat equilibrium position, and it increases with the longitudinal displacement of the central frame. In this DEG, surface stretch variations mainly take place along the meridian direction, whereas the stretch stays nearly constant in the circumferential direction, leading to a deformation kinematics similar to pure shear.^[43] In contrast to conical DE actuators,^[44] which require a mechanical axial preload to produce a stroke (as the flat configuration is a singular configuration), conical DEGs do not strictly require bias mechanisms, thus they can exploit the entire available deformation range. Moreover, cone DEGs can be

arranged in an agonist–antagonist configuration by connecting the central moving discs of two oppositely preloaded coaxial units, hence forming a generator capable of bidirectional forces.^[45]

The circular diaphragm inflatable DEG (Figure 2e) is able to exploit cyclic pressure variations in a fluid. This systems consists in a planar uniformly prestretched circular DEG membrane, whose capacitance is increased upon pressure-induced bubble-like expansion. This topology has been largely investigated due to its simplicity (e.g., there are no moving parts but the DEG membrane) and its ability to reach large area strains, close to the equibiaxial condition, over a large portion of the electrodes surface.^[18,46–48]

Other DEG topologies have been investigated in addition to those presented here. These include, among others: generators which exploit a fluid’s pressure to generate a bubble-like expansion of a tubular DEG membrane;^[49] longitudinally stretched roll (or tube) DEG;^[23,50] and vibro-impact topologies, in which planar DEG membranes are deformed out-of-plane by impact with a vibrating bluff body.^[51]



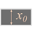
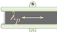

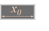
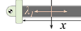

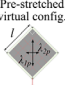
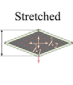


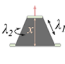



An overview of the features for the different topologies is shown in **Table 1**, which presents information on the deformation kinematics, and the trend of capacitance and convertible energy as a function of the stretches.

2.3. Modeling

Numerical modeling is an important tool to predict the performance of DEGs and design DEGs.

Established modeling approaches for DEGs are available, which describe the electroelastic interactions in DE materials.^[52–54]

Table 1. Overview on the kinematics and geometric generation factor for some DEG topologies.

Topology	Stretch	Capacitance	Generation factor
Equibiaxial Unstretched  Stretched 	$\lambda_1 = x/x_0, \lambda_2 = x/x_0$	$C_{\text{DEG}} = \epsilon \Omega t_0^{-2} \lambda_1^4$	$f_g = 2 \log[(\lambda_1)_C / (\lambda_1)_D]$
Pure shear Unstretched  Pre-stretched  Stretched 	$\lambda_1 = x/x_0, \lambda_2 = \lambda_p$	$C_{\text{DEG}} = \epsilon \Omega t_0^{-2} \lambda_p^2 \lambda_1^2$	$f_g = \log[(\lambda_1)_C / (\lambda_1)_D]$
Uniaxial Unstretched  Stretched 	$\lambda_1 = x/x_0, \lambda_2 = \lambda_1^{-0.5}$	$C_{\text{DEG}} = \epsilon \Omega t_0^{-2} \lambda_1$	$f_g = 0.5 \log[(\lambda_1)_C / (\lambda_1)_D]$
Diamond Unstretched (virtual config.)  Pre-stretched  Stretched 	$\lambda_1 = \lambda_{1p} x / (\sqrt{2}l), \lambda_2 = \lambda_{2p} \sqrt{4l^2 - x^2} / (\sqrt{2}l)$	$C_{\text{DEG}} = \epsilon \Omega t_0^{-2} \lambda_{1p}^{-1} \lambda_{2p} \lambda_1 \sqrt{2\lambda_{1p}^2 - \lambda_1^2}$	$f_g = \log \left[\left(\lambda_1 \sqrt{2\lambda_{1p}^2 - \lambda_1^2} \right)_C / \left(\lambda_1 \sqrt{2\lambda_{1p}^2 - \lambda_1^2} \right)_D \right]$
Conical Unstretched  Pre-stretched  Stretched 	$\lambda_1 = \lambda_p \sqrt{1 + \frac{x^2}{(r_o - r_i)^2}}, \lambda_2 = \lambda_p$	$C_{\text{DEG}} = \epsilon \Omega t_0^{-2} \lambda_p^2 \lambda_1^2$	$f_g = \log[(\lambda_1)_C / (\lambda_1)_D]$
Circular diaphragm Unstretched  Pre-stretched  Stretched 	Tip point: $\lambda_1 = \lambda_2 = \lambda_p (1 + (x/e)^2)$ Perimeter: $\lambda_1 \approx \lambda_p (1 + (x/e)^2), \lambda_2 = \lambda_p$	$C_{\text{DEG}} \approx \epsilon \Omega t_0^{-2} \lambda_p \lambda_1 (\lambda_1^2 + \lambda_p \lambda_1 + \lambda_p^2) / 3$ with λ_1 stretch at the tip ^[47]	Tip: $f_g = 2 \log[(\lambda_1)_C / (\lambda_1)_D]$ Perimeter: $f_g = \log[(\lambda_1)_C / (\lambda_1)_D]$

These models traditionally rely on the following assumptions:
1) Mechanically, the DE layers are described as incompressible hyperelastic composite structures by resorting to rubber elasticity theory.^[55] The effect of strain-dependent mechanical dissipations is considered by means of viscoelastic rheological models, based on which the polymeric materials are rendered as linear networks of hyperelastic elements and dissipative elements.^[56,57]
2) Electrically, the DE material is modeled as a linear dielectric, and the electroelastic interaction is rendered in terms of electrostatic stresses on the DE induced by the electric field (namely, Maxwell stress).^[36] Electrical losses due to the electrodes and the DE material resistivity are accounted for by modeling the DEG as a linear circuit combining capacitive and resistive elements.^[58]

In the following, we recall the fundamental equations that describe the response of a lossless DEG at the local and the global scale.

We first consider a uniform thin electrode-coated local portion of DE membrane subject to in-plane tensile stresses (in a plane-stress condition), as shown in **Figure 3a**.

The deformation of the membrane element is quantified through the principal stretches, which are the ratios between the stretched and unstretched material element lengths along the principal deformation directions. We call λ_1 and λ_2 as the principal stretches on the membrane surface, and λ_3 as the stretch in the thickness direction. As elastomeric materials are incompressible, the following relationship holds

$$\lambda_3 = (\lambda_1 \lambda_2)^{-1} \quad (1)$$

The stress on the DE membrane can be either expressed in terms of the nominal stress (i.e., the force per unit unstretched cross-sectional area) or the real stress (i.e., the force per unit deformed cross-sectional area). Indicating the nominal stresses in the principal directions with s_1 and s_2 , and the principal real stresses with σ_1 and σ_2 , the following relations hold, for which a derivation is presented in Appendix

$$\begin{aligned} \sigma_1 &= \lambda_1 s_1 = \lambda_1 \frac{\partial \Psi(\lambda_1, \lambda_2)}{\partial \lambda_1} - \epsilon E^2, \\ \sigma_2 &= \lambda_2 s_2 = \lambda_2 \frac{\partial \Psi(\lambda_1, \lambda_2)}{\partial \lambda_2} - \epsilon E^2 \end{aligned} \quad (2)$$

where $\Psi = \Psi(\lambda_1, \lambda_2)$ is the strain–energy function, which expresses the volumetric elastic energy density of the membrane as a function of the stretches, according to hyperelastic constitutive relationships;^[55] ϵ is the DE material permittivity; and E is the actual electric field in the DE.

The total stress on a DE membrane is thus the sum of a purely elastic contribution (governed by the constitutive relationships which link Ψ , λ_1 , and λ_2) and an electrostatic compressive contribution referred to as Maxwell stress.^[36] Although different hyperelastic models exist^[55] that use different parameters in the expression of Ψ , an average measure of the elastomer elastic stiffness is provided by the shear modulus, μ_0 . The shear modulus of a material in the reference configuration relates to the energy function as follows^[59]

$$\mu_0 = \lim_{\lambda_1, \lambda_2 \rightarrow 1} \frac{\lambda_1 \frac{\partial \Psi}{\partial \lambda_1} - \lambda_2 \frac{\partial \Psi}{\partial \lambda_2}}{\lambda_1^2 - \lambda_2^2} \quad (3)$$

In the special case in which the DEG geometrical configuration is described by a single degree of freedom (DoF) through a generalized coordinate q , the DEG response is described by the following global equation^[48]

$$F_q = \frac{d}{dq} \int_{\Omega} \Psi(\lambda_1, \lambda_2) d\Omega - \frac{V^2}{2} \frac{dC_{\text{DEG}}}{dq} \quad (4)$$

where F_q is the applied mechanical load acting against q (F_q is a force if q is a linear displacement, it is a torque if q is an angle etc., as shown in Figure 3b), $C_{\text{DEG}} = C_{\text{DEG}}(q)$ is the DEG capacitance and V is the applied voltage. The integral of the strain–energy function is calculated over the total DE volume Ω . Similar to the stresses (Equation (2)), the total DEG load is the sum of two contributions: an elastic restoring force (due to the DE layers elasticity) and an electrostatic contribution (due to Coulomb forces). A derivation of Equation (4) is shown in Appendix.

Most practical DEG topologies shown in Section 2.2 are characterized by simple deformation kinematics, for which the stretches distribution can be estimated as a simple function of the DEG position. Their response can be thus studied by applying Equation (4). Table 1 shows the in-plane stretches λ_1 and λ_2 for the topologies discussed in Section 2.2. It is assumed that the considered DEG configurations are described by a single geometric coordinate, and simplified distributions for the principal stretches on the electrodes surface are presented accordingly. In particular, in the equibiaxial and pure-shear case, necking

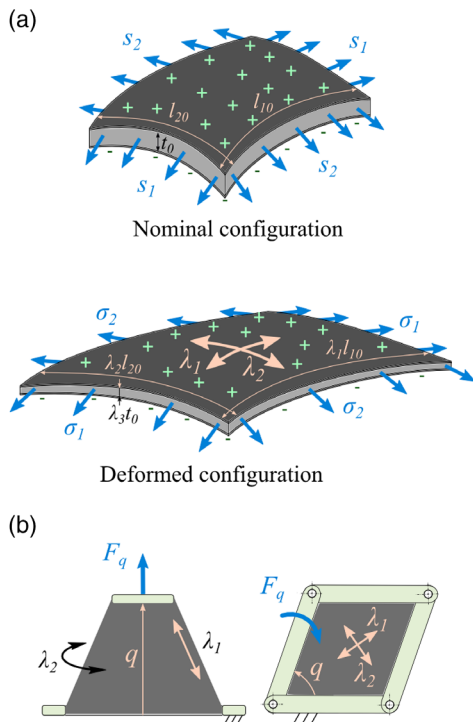


Figure 3. a) A patch of electrode-coated DE membrane subject to uniform stress, strain, and electric field. The top picture shows the DE patch in the undeformed (nominal) state, whereas the bottom one shows the actual deformed membrane. b) Example of DEG topologies whose deformation kinematics can be rendered by a single generalized coordinate q , subject to an external generalized load F_q .

effects due to a multipoint stretching mechanism (Figure 2a) or to free edges are neglected. In the diamond DEG, the stretches on the DE membrane are assumed uniform, and prestretches are mathematically defined as the stretches achieved in the square configuration (though this configuration might not be part of the actual device working range).^[39] In the cone DEG, meridian necking of the membrane is neglected and the stretches are assumed uniform throughout the DEG.^[43] In the circular diaphragm DEG, stretches are nonuniform (they are maximum at the tip point), and reduced models have been proposed to describe their distribution.^[47] The capacitance C_{DEG} is calculated assuming that each DEG has a single layer of DE material coated by electrodes.

In addition to establishing relationships between the deformation, the applied voltage, and the mechanical loads, analytical models provide a means of estimating the energy that a DEG provides in a conversion cycle and its maximum convertible energy.

2.4. Maximal Convertible Energy

Knowledge of the deformation kinematics of a DEG and assumptions on the physical operating limits allow the estimation of the maximum energy which can be converted in a cycle.

The following set of physical operating limits holds for a DEG:^[31,32] 1) mechanical rupture (MR) of the DEG, which sets an upper bound to the maximum stretch which can be safely applied; 2) the dielectric strength of the DE material, i.e., the maximum admissible electric field that can be applied across the DE before dielectric breakdown (BD); 3) electromechanical instabilities (EMIs), including the loss of mechanical tension due to the electrostatic stress (i.e., the stresses in Equation (2) falling to zero due to Maxwell stress) and positive-feedback deformation–voltage variation patterns.^[53] The set of the physically admissible states for a DEG can be represented either on a charge–voltage Q – V diagram or on a force–position F_q – q diagram (with reference to the generalized coordinate and load defined in Section 2.3) as a closed region bounded by a set of limit curves representing the different failure mechanisms. In particular, on the diagrams shown in **Figure 4**, lines (B)–(C) represent fixed-configuration isocapacitance curves in which the DEG is stretched up to the MR condition; curves (C)–(C') and (C')–(D) represent the limit states where the DEG experiments BD or EMI. In addition to the limit curves, line (A)–(B) on the q – F_q plane represents the DEG force during stretching (when no voltage is applied), whereas lines (D)–(A) correspond to the configuration where the DEG reaches the minimum capacitance achievable due to geometric constraints. The envelope of the feasible region corresponds to a limit cycle, namely (A)–(B)–(C)–(C')–(D)–(A), following which the DEG can theoretically deliver the maximum convertible energy per cycle. With reference to the four-phase cycle shown in Figure 1a, (A)–(B) corresponds to stretching phase (P1), (B)–(C) to priming phase (P2), (C)–(C')–(D) to generation phase (P3), and (D)–(A) to discharging phase (P4). The electrical energy generated in a cycle is equal to the area of the limit cycle on the Q – V plane. In the absence of electromechanical losses, this equals the input mechanical energy, corresponding to the area of the limit cycle on the q – F_q plane.^[31]

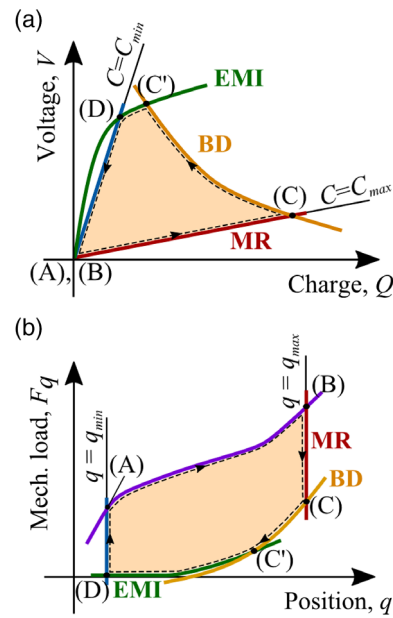


Figure 4. a) Charge–voltage diagram and b) generalized force–displacement diagram showing the limit curves relative to the DEG failure mechanisms and the feasible working space.

To evaluate the parameters which affect the convertible energy of a DEG, we hereby introduce the following simplifications: 1) the distribution of the stretches on the DE membranes is uniform; 2) the DEG deforms between two limit configurations (state (C) and (D) in Figure 4a), without being affected by any EMI (i.e., (C') coincides with (D)); 3) the BD electric field for the DE, E_{BD} , is a constant and is independent of the stretch. With these assumptions, the energy converted by the DEG throughout cycle (A)–(B)–(C)–(D)–(A) is given by

$$W_e = \varepsilon \Omega E_{\text{BD}}^2 f_g, \quad \text{with} \quad f_g = \log \frac{(\lambda_1 \lambda_2)_{(C)}}{(\lambda_1 \lambda_2)_{(D)}} \quad (5)$$

where Ω is the total (constant) DE volume and ε is the DE permittivity. The derivation of Equation (5) is discussed in Appendix. According to Equation (5), the convertible energy is proportional to $\varepsilon \Omega E_{\text{BD}}^2$ (i.e., the volumetric energy density is proportional to $\varepsilon E_{\text{BD}}^2$), and a factor f_g (hereafter called the generation factor) which depends on the surface stretch ratio between configurations (C) and (D). Factor f_g only depends on the DEG geometry, and it changes by changing the DEG topology. Table 1 shows an estimate of the generation factor f_g for some relevant DEG topologies. The conversion factor f_g is expressed as a function of the ratio of stretch λ_1 in two different configurations (i.e., a higher stretch configuration (C) and a lower stretch configuration (D), as shown in Figure 1a). Equibiaxial deformation maximizes the generated energy, which theoretically amounts to two times that achieved with pure-shear deformations (assuming same values for the maximum/minimum stretch during operation). The generation factor with uniaxial stretch (i.e., simple elongation) is 1/2 that of pure shear and 1/4 that of the equibiaxial case, hence making the uniaxial topology of scarce interest for DEGs. The

conical layout leads to a theoretical stretch distribution (and, hence, a generation factor) equal to that of pure shear, whereas in the diamond DEG f_g is strictly lower than for pure shear, due to the reduction in the transverse stretch upon longitudinal loading. Finally, the inflating circular diaphragm DEG implements a deformation kinematics which is intermediate between pure-shear (which takes place at the membrane clamped edge) and equibiaxial deformation (at the membrane centre), with the second being predominant over a significant portion of the membrane surface in the case of highly deformed DEG bubbles.^[46]

Based on Equation (5), the maximum applied electric field is key to achieve large convertible energy densities. Electric fields on the order of 10^1 – 10^2 kV mm⁻¹, consistent with the typical BD strength of DE materials,^[60,61] result in energy densities on the order of 10^{-1} – 10^0 J cm⁻³. To achieve such figures, however, the application of large voltages is required, unless extremely thin DE layers are manufactured. Assuming DE layer thickness on the order of tens or hundreds of micrometers (consistently with available scalable manufacturing processes),^[60] the resulting operating voltages are on the order of 1–10 kV. From a technological standpoint, the deployment of practical DEG systems requires effort either toward the development of bidirectional high-voltage power electronics (Section 3), or the manufacturing of stacks with micrometer-thick DE layers suitable to operate at lower voltages.

The efficiency and convertible energy of a DEG is limited by electromechanical loss mechanisms. The global efficiency of a DEGS further depends on the efficiency of its driving electronics. DEG mechanical losses mainly consist in rate-dependent viscous losses^[56] that increase proportionally with the strain rate, although some DE materials also exhibit a pseudoelastic behavior characterized by rate-independent hysteresis.^[61,62] If the dissipated-to-stored mechanical energy ratio for a DE material is high, mechanical losses cause a significant drop in the DEG efficiency, though they do not inhibit a DEG's ability to produce a positive electrical power output and do not affect the maximum convertible electrical energy density. DEG electrical losses are due to the R – C dynamics within the DEG, and they lead to reductions in both the DEG efficiency and the convertible energy density. These include: 1) leakage currents through the dielectric layers due to the finite DE material resistivity; 2) voltage inhomogeneities over the electrodes, due to the finite conductivity of the compliant electrode materials.

Due to leakage currents, part of the generated electrical energy is dissipated by the Joule effect through the DE layers. Indicating with κ_d the DE material conductivity, the energy dissipated by leakage currents can be considered negligible compared to that harvested by the DEG if time constant $\tau_d = \epsilon/\kappa_d$ is significantly larger than the generation cycle duration. Time constant τ_d is a material property of the DE, and it quantifies the DEG self-discharging characteristic time due to the material conductivity, regardless of the DEG topology.^[61]

Due to non-negligible electrode resistivity, the electric field on some portions of the DE material (far from the connections with the power electronics) might result in being lower than the target static value, limiting the DE material capability to uniformly achieve large convertible energy densities.^[63] Indicating with R_s the sheet resistance of the compliant electrodes, the characteristic R – C time constant of the electrodes-DE assembly is

$\tau_e = R_s C_{\text{DEG}}$. In contrast with τ_d , time constant τ_e depends on both the DEG system dimensions and the materials properties, and it is required to be as small as possible. With reference to the four-phase operating cycle introduced in Section 2.1, in particular, τ_d should be significantly smaller than the typical duration of phases ($P2$) and ($P4$), so as to prevent significant losses by Joule effect during the priming and the discharging transients.

The maximum convertible energy and efficiency of a DEG strongly depend on material properties. In addition to featuring large permittivity and BD field (which lead to large convertible energy density), DE materials for DEGs should provide limited electromechanical losses, especially in those applications where efficiency is paramount (e.g., large-scale power production). Compliant electrodes should implement low sheet-resistance and keep their properties unchanged upon large cyclic stretching.

2.5. Materials

Dielectrics commonly used in DEGs include: 1) acrylic elastomers, in particular, commercial adhesive tape VHB by 3M, which is largely used to build laboratory demonstrators;^[19,45,46,64] 2) natural or synthetic (e.g., styrene-based) rubber;^[18,39] and 3) silicone elastomer (polydimethylsiloxane).^[24,65,66]

Acrylic VHB tape has been largely used for DE demonstrators due to its ability to adhere to substrates and its chemical compatibility with commercial conductive grease/paste, which make prototypes manufacturing particularly convenient. Nonetheless, this material has high electromechanical losses and limited reliability upon cyclic loading.^[67] Natural rubber has been indicated as a promising DE for energy scavenging applications due to its large BD strength.^[18,31] Dielectric properties similar to those of natural rubber have been recently observed also in styrene-based synthetic rubber, whose application in DEGs is to date barely explored.^[61] Silicones are regarded as strategic for future DE applications as they can be processed following different manufacturing techniques^[68,69] and offer room for electromechanical properties improvement via physicochemical modification of their components.^[60]

Table 2 shows an overview of the material properties of three commercial elastomers, taken as representatives of the above mentioned DE categories (acrylic, rubber, and silicone). These materials are: acrylic VHB 4905 by 3M; natural rubber Oppo Band Green 8003 by Oppo; and Elastosil silicone (in particular, Elastosil 2030 films) by Wacker Chemie AG. VHB acrylic is commercialized as a tape, whereas Oppo Band is commercialized as an exercise band, i.e., both these materials are not specifically conceived for DE applications. Elastosil silicone has been originally commercialized as a general-purpose raw material, though recently high-tolerance thin films have been also produced purposely for DE application.^[70]

The properties of VHB, and Oppo Band in Table 2 were obtained by Chen et al.^[61] Unless otherwise referenced, the properties of Elastosil silicone refer to Elastosil 2030 films and they have been measured here using setups and procedures similar to those described in the study by Chen et al.^[61] The shear modulus and the mechanical loss refer to pure-shear tensile tests with maximum strain equal to roughly 90% the elongation at break

Table 2. Electromechanical properties of three reference commercial DE materials.

	Acrylic VHB 4905 ^[61]	Oppo Band Green rubber ^[61]	Elastosil silicone
Shear modulus, μ_0 [kPa]	17	620	308
MR stretch (pure-shear test)	8.2	5.2	5.5 ^[70]
Relative permittivity ^{a)} , ϵ/ϵ_0	4.14	2.74	2.85
BD strength, E_{BD} [kV mm ⁻¹]	70–180	100–300	75–195 ^[71,72]
ϵE_{BD}^2 [J cm ⁻³]	0.2–1.2	0.2–2.2	0.1–1.0
Conductivity, κ_d [$\mu\text{S m}^{-1}$]	1–5	0.1–0.4	5×10^{-4} – 5×10^{-2}
$\tau_d = \epsilon/\kappa_d$ [s]	7–37	60–242	500–50 000
Mech. loss [%]	12–17	4–23	2–4

^{a)} $\epsilon_0 = 8.85 \text{ pF m}^{-1}$ is the vacuum permittivity.

and strain rate between 0.08 and 0.8 s⁻¹; the BD electric field ranges account for different applied stretches or voltage waveforms during the tests; the conductivity is measured at different applied electric fields between 10 and 80 kV mm⁻¹.

In addition to large permittivity and stretchability, VHB acrylic has significantly lower elastic modulus μ_0 compared with other DEs. In applications, this allows the achievement of large DEG deformations with limited input forces and with no need for external static or dynamic negative-spring mechanisms for DEG's stiffness compensation.^[44,61,73] Nonetheless, this elastomer has large hysteresis losses and non-negligible electrical conductivity, which limit the efficiency and the convertible energy in practical applications. The value of self-discharging time constant τ_d suggests that this material is unsuitable for low-frequency applications (on the order of 10⁻¹ Hz).

Oppo Band has a remarkably larger BD strength (up to 300 kV mm⁻¹ in the stretched state) and significantly lower conductivity than acrylic. This material also has a rather large maximum mechanical loss at large strains (up to 470%), though it has demonstrated significantly lower viscous losses than VHB at intermediate stretches (below 400%).^[61] Compared with synthetic elastomers, natural rubber has a low carbon footprint^[74] and it is biodegradable,^[75] hence offering a relevant option for future environmentally aware markets. Rubber is to date scarcely applied in DEs.^[18,39] This is due to the large thickness of commercial films (above 200 μm), which creates a demand for inconveniently high operating voltages.

Elastosil silicone holds elastic modulus, dielectric constant and elongation at break similar to those of rubber, and maximum measured BD field of 195 kV mm⁻¹.^[71] Based on the product ϵE_{BD}^2 , natural rubber appears virtually capable of larger convertible densities than silicone within a same stretch range. However, a systematic characterization of the BD strength at different stretches is currently missing for Elastosil, hence making a reliable comparison not particularly significant. Remarkably, Elastosil silicone shows lower mechanical losses (2–6 times) and extremely lower conductivity (1–4 orders of magnitude) than VHB and rubber. Therefore, it bears the potential to perform efficiently even in the low-frequency range below 1 Hz.^[65]

In addition to commercial films, custom silicone elastomers have been synthesized with the aim of improving the BD strength, the permittivity, the tensile strength, or reducing the elastic modulus.^[60] Particular attention has been put into the synthesis of high permittivity elastomers through the addition of high-permittivity matter in the silicone matrix,^[76,77] blending in high-permittivity oils,^[78] or chemical modification of the silicone backbone.^[79] Thriving ongoing research in material science seems to suggest that silicones might gain a leading role in the DE panorama in the next few years.^[60]

As regards materials for compliant electrodes, carbon-loaded grease has been largely used in laboratory prototypes, especially in combination with acrylic dielectrics.^[19,46,64,80] Although this solution is practical for prototypes (electrodes are simply painted on the DE layers), it does not provide stable and durable electrodes for real-world applications. Candidate materials for applications^[68] are conductive elastomer layers doped with conductive fillers,^[68] and sputtered micrometer-thin metal films.^[81] Manufacturing of carbon-loaded polymeric electrodes has been proven using silicone as the base elastomer and carbon black, carbon nanotubes, or graphene as the fillers,^[60] leading to sheet resistances in the range 50 $\Omega \text{ sq}^{-1}$ –20 k $\Omega \text{ sq}^{-1}$.^[65,82]

In the case of silicone transducers, integrated manufacturing of composite dielectric–electrode membrane assemblies has been demonstrated via pad printing,^[68] blade casting,^[65] screen printing,^[69] and inkjet printing.^[83]

In addition to dielectric and electrode properties, a relevant performance index for DEGSs is the number of electromechanical cycles that they can withstand. Lifetime of DE transducers has been mostly studied with reference to actuators,^[84–86] with a few works specifically referring to DEGSs.^[49,67]

Silicone-based DE actuators have been reported to achieve maximum lifetimes over 10⁸ cycles.^[84] Despite exploiting similar peak electric fields to DE actuators (in the same order of magnitude as the BD field), generators are typically subject to larger strain variations, therefore they are potentially more prone to combined electromechanical aging. Lifetime of DEGSs is influenced both by the ability of a DE material to resist to a large number of cycles prior to BD, and by the electrodes' ability to guarantee electrical continuity upon large-strain cycles.

As regards DE materials' fatigue life characterization, separate researches have been conducted to assess the lifetime upon mechanical stretching (without applied voltage),^[67] or upon cyclical charging–discharging (at fixed stretch).^[87–89] Numerous studies on the mechanical fatigue life of natural and synthetic rubbers exist, which suggest that mechanical life on the order of 10⁶–10⁸ cycles can reasonably be expected.^[90–92] By studying the crack propagation in thin films subject to pure shear, Jean-Mistral et al.^[67] concluded that Elastosil silicone films have fatigue properties similar to rubber, and significantly better than VHB acrylic.^[93] Chen et al. studied lifetime upon electrical loading at constant stretch for a commercial synthetic rubber band^[87] and for Elastosil 2030 films.^[88] At electric fields on the order of 70–75 MV m⁻¹ and frequency of 1 Hz, the mean number of cycles to failure was 10⁴ for rubber and over 2 \times 10⁶ for silicone. Beyond materials properties, this difference is ascribable to the different manufacturing quality of the two films. Commercial films not specifically produced for DE applications (like most acrylic and rubber films) rely on simple processes which

guarantee low material cost but lead to scarce durability in DE applications. Guaranteeing appropriate quality of DE films manufacturing seems key to reach lifetimes consistent with DEGS requirements.

As regards electrodes lifetime, de Saint-Aubin et al.^[85] observed that inkjet-printed electrodes and stamped silicone-carbon composites can guarantee lifetimes on the order of 10^7 cycles (as opposed to 10^5 cycles of manually painted electrodes) at strains of a few points percent. Electrodes lifetime in the presence of large strains ($>200\%$) is to date barely explored, and might represent a bottleneck as relevant as the dielectric material lifetime.

Dedicated research on DEG failure mechanisms, electromechanical aging and compliant electrodes durability upon stretching will be key, in the near future, to provide research directions for DEG materials and manufacturing.

3. Electronics

3.1. Laboratory Electronics

Because DEGs do not generate charges, even the most basic implementation of a harvesting cycle, such as shown in Figure 1, requires a companion electronic circuit that loads and unloads charges on the DEG in synchronization with the mechanical cycle. This section reviews basic electronic circuits that are commonly used in a laboratory environment to test and characterize generators. They are designed to evaluate the achievable performance of DEGSs and to study their behavior in different operating conditions, and not to store the generated energy and/or step it down to usable voltages.

3.1.1. Circuit for Rectangular Cycles

The simplest electronic circuit for the priming of DEGs is shown in Figure 5 and consists of a voltage source V_L , 2 diodes, and a very large capacitor charged at a voltage $V_H > V_L$. In addition to its simplicity, this circuit has the advantage of not requiring switches to synchronize the electrical cycle on the mechanical cycle, because the diodes act as self-synchronizing voltage-activated switches. The harvesting cycle in the charge–voltage (Q – V) plane is shown in Figure 5b. When the DEG is stretched and its capacitance increases ((A)–(B)), charges are free to flow from the source V_L to the DEG, whose charge level increases from Q_{\min} to Q_{\max} at voltage V_L . When the DEG starts relaxing, its capacitance decreases, leading to an increase in voltage ((B)–(C)). As D_1 and D_2 are both reverse polarized, the charges are trapped on the device until its voltage reaches V_H . At this point D_2 conducts, and charges flow from the DEG into the infinitely large storage capacitor C_s at a constant voltage (CV), until the DEG is completely relaxed ((C)–(D)). When the DEG starts stretching again, its voltage decreases until it reaches V_L ((D)–(A)) at which point D_1 conducts again and enables charging of the DEG from the external supply. During one cycle, the voltage source provides an electrical energy $W_{\text{in}} = V_L(Q_{\max} - Q_{\min})$, and the energy transferred to the output capacitor is $W_{\text{out}} = V_H(Q_{\max} - Q_{\min})$, for a net energy gain $W_e = (V_H - V_L)(Q_{\max} - Q_{\min})$, representing the surface of the

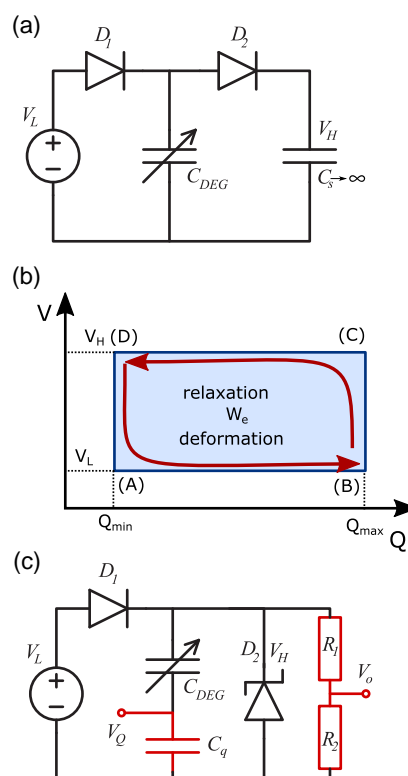


Figure 5. a) Constant-charge–constant-voltage (CCCV) circuit for a DEG. The voltage source V_L charges the DEG through D_1 and the DEG discharges through D_2 into an infinitely large storage capacitor C_s at voltage $V_H > V_L$. b) Behavior of the circuit on a Q – V plot, with the surface of the rectangle being the net electrical energy W_e harvested during a cycle. c) In practice, the infinitely large capacitor is usually replaced by a Zener diode with BD voltage V_H . The components in red are added to measure the performance of the DEG.

rectangle in the graph shown in Figure 5b. Harvesting cycles are usually named according to the DEG state during the relaxation phase, and this circuit enable a constant-charge–constant-voltage (CCCV) cycle and can be referred to as the CCCV circuit.

In practical implementations of the circuit, the infinitely large capacitor is usually replaced by a Zener diode with a BD voltage V_H ^[26,33] (Figure 5c); the fact that the output energy is dissipated rather than stored is usually unimportant for laboratory set-ups aimed at characterizing the output performance of DEGs. However, implementations using capacitors, both for the low-voltage source and the high-voltage sink, have also been implemented.^[18] Additional components can be added to measure the Q – V behavior of the generator. A possible implementation based on the work of McKay et al. is shown in Figure 5c, with the components required for the characterization highlighted in red.^[26] Resistances R_1 and R_2 form a resistive divider with a high impedance to step down the output voltage of the DEGs to a few volts with a minimum current leak. C_q is a large capacitor which is used as an integrator with an output voltage V_Q proportional to the amount of charges Q on the DEG. As an alternative to the capacitor C_q , the charge on the DEG can also be calculated by integration of the current flowing to the DEG.^[33]

The energy-harvesting system shown in Figure 5 has four main parameters: the initial capacitance C_{\min} of the undeformed device, the maximal capacitance swing of the DEG $\beta_{\max} = C_{\max}/C_{\min}$ (with C_{\max} being the capacitance at maximal deformation) which depends on the amount of deformation of the generator, and the two voltage levels V_H and V_L . McKay et al. have shown that the harvested energy can be maximized while keeping the electric field below a maximal value E_{\max} , if^[26]

$$V_H = E_{\max} \frac{\Omega}{S_{\min}} \frac{1}{\sqrt{\beta_{\max}}} \quad (6)$$

$$V_L = \frac{1}{\sqrt{\beta_{\max}}} V_H \quad (7)$$

with Ω as the volume of active DE material, and S_{\min} as the surface of the DEG capacitor in its minimum capacitance state, i.e., at point (D) of the cycle. Using these voltage values leads to the following amount of net generated electrical energy per cycle

$$W_e = \varepsilon E_{\max}^2 \Omega \left(1 - \frac{1}{\sqrt{\beta_{\max}}}\right)^2 \quad (8)$$

Due to its simplicity, and ease of implementation, this approach has been used in several investigations centered around the amount of energy that can be harvested by DEGs.^[18,33,46,56,56,94]

3.1.2. Circuit for Triangular Cycles

With optimal parameters, the simple circuit of the previous section produces a cycle equal to the largest rectangle that can be placed within the feasible area of Figure 4a. However, given the shape of the available energy surface, a triangular cycle would enable to harvest more energy. This is made possible by the circuit shown in **Figure 6**. It consists of a current source I_{in} , the DEG C_{DEG} , a storage capacitor C_s , and a load R_L that represents some harvesting circuit. Two switches and a diode separate the different elements (Figure 6a). Depending on the value of the storage capacitor C_s , different triangular cycles can be obtained: CC, CV, or an optimal cycle approaching the constant electric field (CE) case. The terms apply to the condition of the DEG during the relaxation phase (segment C–D, Figure 6b). With this driving circuit, the source of priming charges should be a current source so that the output voltage can adapt to the charge level of the DEG. If a CV source is used instead, the amount of required input energy would double, with the additional contribution dissipated in the internal resistance of the source. In practice, for testing purpose in the lab, the energy possibly dissipated by the priming source can usually be ignored.

We first describe the operation of the circuit for the optimal value of C_s , as shown in Figure 6b.^[19] At the beginning of the cycle (A), both the switches are open and both the capacitors are discharged. The DEG is mechanically stretched from its minimal capacitance C_{\min} to maximal capacitance C_{\max} (B). Then, S_1 is closed and the external source charges the DEG and C_s until the voltage reaches V_{in} , at which point S_1 is opened again (C). The DEG is then mechanically relaxed to its minimal capacitance C_{\min} (D). This causes its voltage to increase, and a transfer of

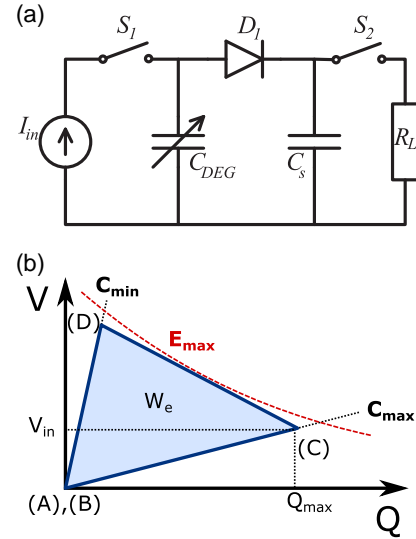


Figure 6. a) Circuit for a triangular harvesting cycle. b) Harvesting cycle obtained with the circuit shown in the Q - V plane. The slope of segment C–D is set by the value of capacitor C_s .

charges from the DEG to C_s to take place through D_1 . The slope of line C–D is inversely proportional to C_s (i.e., $V = -1/C_s(Q - Q_{\max}) + V_{in}$), which means that the voltage V_{in} at which the DEG is charged and the value of capacitance C_s can be chosen so that the segment C–D of the cycle becomes tangent with the Q - V curve describing the maximal electric field tolerated in the device. Finally, the switch S_2 is closed and the charges stored in C_s , as well as the remaining charges on the DEG, are collected by a harvesting circuit or dissipated through a load in a laboratory setting (back to (A)).

To obtain the optimal triangle (OT) cycle, as drawn on Figure 6b, segment C–D must be tangent to the curve that describes maximal admissible electric field (red curve). This can be achieved if the storage capacitance is chosen to be $C_s = \sqrt{\beta_{\max}} C_{\min}$, and if the switch S_1 is opened when the voltage on the DEG reaches

$$V_{in} = \frac{E_{\max} \Omega}{S_{\min}} \frac{2}{\sqrt{\beta_{\max}} + \sqrt[4]{\beta_{\max}}} \quad (9)$$

with Ω as the volume of the generator active material, S_{\min} as the surface of the generator in its minimal capacitance state, i.e., at points (A), (B), and (D) of the cycle. This cycle approaches a CE cycle, for which the electric field of the DEG remains constant during relaxation. An exact CE cycle would include the complete area defined by the two isocapacitance lines and the E_{\max} curve. It requires active control of the voltage of the DEG during relaxation, and calls for more complex driving electronics, which is usually not implemented in a research laboratory environment. However, CE cycles enable to harvest more energy and are of interest for high-power harvesting systems (c.f. Section 3.3).

In addition to the optimal value of the storage capacitance C_s , two other particular values of C_s are of interest. In case the capacitance C_s is zero (i.e., C_s and D_1 are removed from the circuit),

the segment C–D becomes vertical, and a CC cycle is obtained. If C_s is infinite, segment C–D becomes horizontal, and a CV cycle is achieved. **Figure 7a–d** shows the optimal cycle for each of these three triangular cycles, as well as the for the CCCV cycle from the previous section. It also reports the voltage thresholds between each segment of the cycles, with Ω as the volume of the generator active material, S_{\min} as the surface of the generator in its undeformed state, and β_{\max} as the maximal capacitance swing. For each cycle, the hatched area represents the amount of input energy required to prime each cycle.

Based on the work from Graf et al.,^[95] we calculate the volumetric energy density w_e harvested per cycle (colored area), the energy density provided by the priming source (hatched area),

and the ratio between the two (**Table 3**). The energy densities of each cycle have a common factor ϵE_{\max}^2 . **Figure 7e** shows the normalized energy density $w_e/(\epsilon E_{\max}^2)$ as a function of the maximal capacitance swing β_{\max} . The CE cycle is producing the maximum energy per cycle but cannot be obtained with a simple driving circuit. However, the difference with the OT cycle is negligible. Third comes CC and CV (same value of w_e), and finally, the CCCV cycle generates the lowest amount of energy. Another important metric is the ratio of harvested energy with respect to the input energy provided by the external source^[95] (**Table 3**, column 4 and **Figure 7f**). The lower this ratio is, the more efficient the electronic circuit (priming, harvesting, stepping down) must be, or there is a risk that the energy available

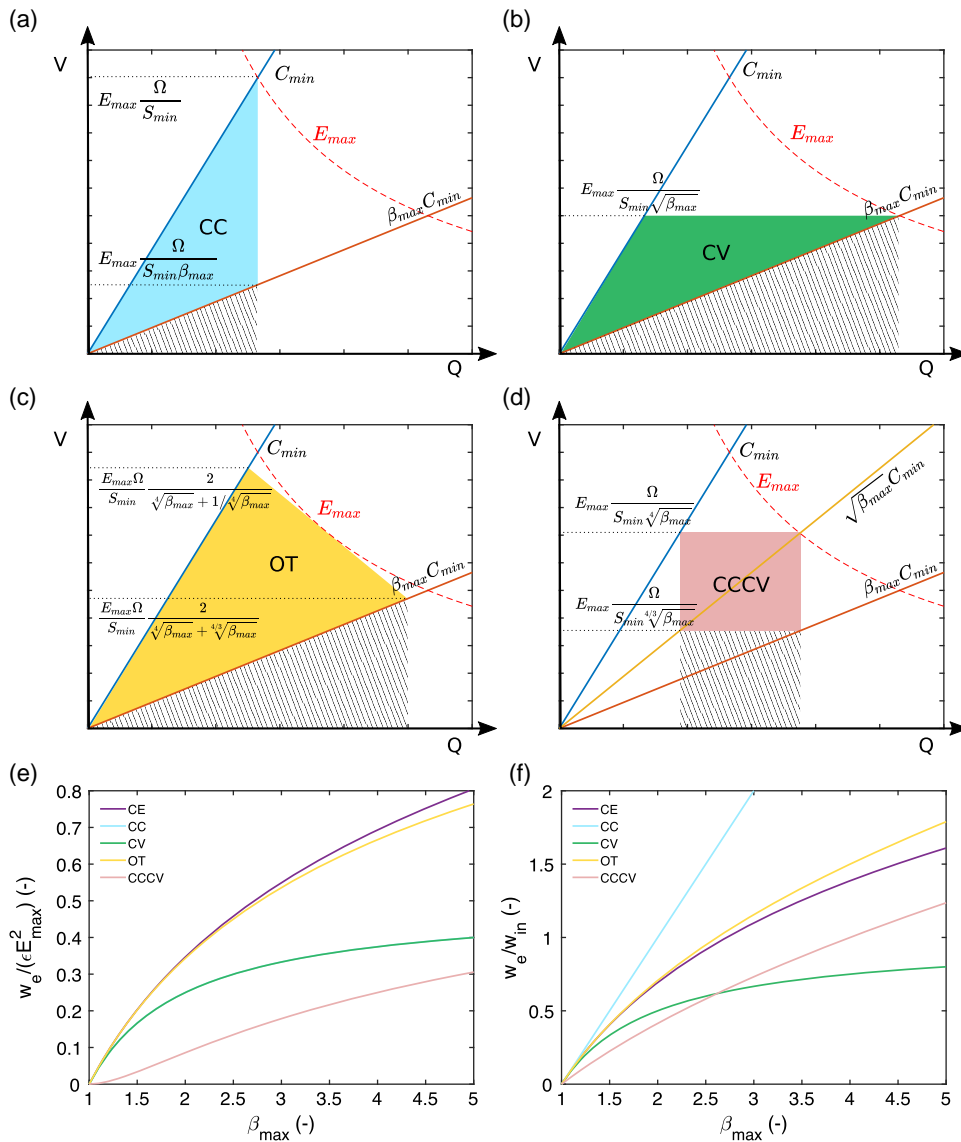


Figure 7. a–d) Different energy harvesting cycles in the Q – V plane: CC, CV, OT, and CCCV. The hatched areas represent the amount of input energy requested for each cycle, and the colored areas represent the net energy gain. e) Relative energy density as a function of maximal deformation. CC and CV curves are overlapping. f) Ratio of harvested energy density versus electrical energy density input. For (e) and (f), the values for a true CE cycle are given for comparison.

Table 3. Generated energy density w_e per cycle, input energy density per cycle w_{in} , and ratio between the generated and input energy densities $w_e/w_{in} (-)$ for the five different cycles. ϵ is the dielectric constant of the membrane, E_{max} is the maximal electric field at which the DEG is operated, and β_{max} is the capacitance swing at maximal deformation.

Cycle	w_e [$J m^{-3}$]	w_{in} [$J m^{-3}$]	$w_e/w_{in} [-]$
CE	$\epsilon E_{max}^2 \ln(\sqrt{\beta_{max}})$	$\frac{1}{2} \epsilon E_{max}^2$	$2 \ln(\sqrt{\beta_{max}})$
CC	$\frac{1}{2} \epsilon E_{max}^2 (1 - \frac{1}{\beta_{max}})$	$\frac{1}{2} \epsilon E_{max}^2 \frac{1}{\beta_{max}}$	$\beta_{max} - 1$
CV	$\frac{1}{2} \epsilon E_{max}^2 (1 - \frac{1}{\beta_{max}})$	$\frac{1}{2} \epsilon E_{max}^2$	$1 - \frac{1}{\beta_{max}}$
OT	$2 \epsilon E_{max}^2 \frac{\sqrt{\beta_{max}-1}}{\sqrt{\beta_{max}+1}}$	$\epsilon E_{max}^2 \frac{2}{2 + \sqrt{\beta_{max}+1} + \sqrt{\beta_{max}}}$	$\frac{\beta_{max}-1}{\sqrt{\beta_{max}}}$
CCCV	$\epsilon E_{max}^2 (1 - \frac{1}{\sqrt{\beta_{max}}})^2$	$\epsilon E_{max}^2 \frac{1}{\sqrt{\beta_{max}}} (1 - \frac{1}{\sqrt{\beta_{max}}})$	$\sqrt{\beta_{max}} (1 - \frac{1}{\sqrt{\beta_{max}}})$

after deduction of the losses ends up being less than the energy provided by the priming source. Although the CC and CV cycles produce the same amount of energy per cycle, the CC cycle requires a much smaller energy input, and is therefore the best in terms of energy delivered versus priming energy.

Although the operational theory of the circuit shown in Figure 6 leads to a triangular cycle, the experimental data from Shian et al. on a soft acrylic elastomer shows a flatten corner at (D), which decreases the effective harvested energy.^[99] This can be attributed to loss of mechanical tension in the membrane due to the viscoelasticity, as modeled by Fan et al. using a dissipative DEG model.^[96] Based on this observation, Fan and Chen have proposed a slightly modified version of the circuit shown in Figure 6, replacing S_2 with a three-way switch connected to Zener diodes with different BD voltages, which enables the generation of a trapezoid cycle.^[97] They have used the data from Shian et al. to simulate the expected energy harvested with the trapezoid circuit and obtained an increase in 6.6% in the generated energy density.

3.1.3. The Need for Self-Sensing

Circuits with switches rely on their timely operation to harvest energy optimally. Conditions for switch operation usually depend on the stretch state, or voltage on the DEG. For example, the switch S_1 of Figure 6 must close when the DEG reaches maximal deformation, and open once the voltage on the DEG reaches V_{in} . Activation of a switch when the DEG reaches its maximal or minimal stretch can be difficult to implement mechanically when the deformation amplitude is not well controlled and varies between cycles (e.g., in human body motion, or wave energy harvesting). However, capacitive self-sensing, which consists in measuring the capacitance of dielectric transducers while deformed or actuated,^[98] can be applied to DEGs to determine the capacitance of the generator, while it undergoes deformation. For example Zanini et al. have proposed a self-sensing scheme which measures the capacitance of a DEG while it is connected to the charging circuit, and estimates it for the rest of the cycle.^[99] They implemented a robust peak-detection algorithm based on a sliding-mode differentiator to determine when the DEG reaches the maximal and minimal capacitance states. This information can then be used to control the activation of the switches at

the optimal time, and is able to adapt to a varying deformation amplitude between cycles.^[99]

3.2. Electronics for Distributed and Wearable Applications

The circuits of Section 3.1 are well-adapted to generate optimal cycles in a laboratory environment. However, they suffer from two important drawbacks that render them difficult to integrate in a real-world application. First, some of the operating parameters of these circuits depend on the capacitance swing of the generator. Once the circuit components are fixed, a well-defined and constant stretching cycle is required to harvest the maximum amount of energy. However, most practical usage scenarios of DEGSs (c.f. Section 4) lead to a nonconstant deformation amplitude. To give one example, a DEG integrated in the heel of a shoe sees its compression state change depending on the weight of the users, their pace, and the terrain. Even the simple CCCV circuit, which does not rely on active switches (Figure 5) has parameters (namely the two voltage levels) that depend on the capacitance swing, i.e., the amount of deformation. Consequently, a varying maximal capacitance swing β_{max} would require on-the-fly adaptation of the input and output voltage levels. A self-sensing scheme can be used to mitigate that issue,^[99] but at the cost of a more complex implementation. The second important limitation of these circuits is that they require an input of electrical energy at each cycle. This may not be problematic for high-power systems connected to the grid, provided that bidirectional power converters are put in place. However, this represents a severe limitation for wearable or distributed systems, for which such circuit topologies only provide an enhancement of battery life, rather than removing the need for a battery. The following sections examine alternative circuits for the priming of DEGs that address the limitations we just mentioned.

3.2.1. The Self-Priming Circuit

The self-priming circuit (SPC) was introduced by McKay et al.^[64] It consists of a circuit, which is able to convert a quantity of electrical energy from a low-charge–high-voltage configuration to high-charge–low-voltage. The DEG transfers charges at high voltage to the SPC when it relaxes, and the SPC returns more charges at a lower voltage to the DEG when it stretches. This back and forth exchange of charges enables to gradually increase the quantity of charges and the voltage of a DEG. The SPC differs from the circuits shown in Section 3.1 on two important points: 1) it does not require an external electrical energy input at each cycle, although it still requires an initial small amount of charges to get started, and 2) energy is not harvested at each cycle, but only once the voltage on the DEG has reached a threshold.

In its most simple embodiment (first-order SPC), an SPC consists of two capacitors of equal value C , and three diodes, as shown in Figure 8a. Depending on the voltage state of the different branches of the circuit, the diodes will be polarized differently, leading to three states of the circuit (Figure 8b–d). For simplicity, we consider the diodes to act as perfect switches. When the three diodes are reverse polarized, the circuit is interrupted, and no charge flow occurs (Figure 8c). When diode D_2 conducts the two capacitors of the SPC are in series, with a total

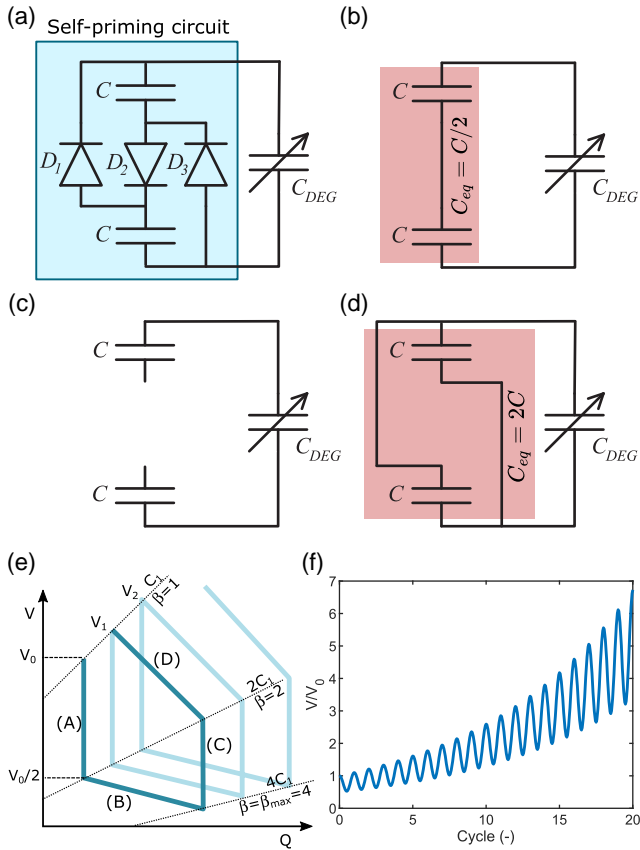


Figure 8. a) A first-order SPC connected to a DEG. It consists of two capacitors of equal value C , and three diodes. Depending on the voltage of the circuit, it can take the following configurations (diodes considered as ideal switches): b) series configuration with an equivalent SPC capacitance of $C/2$ when D_2 is conducting, c) open-circuit configuration when all diodes are reverse biased, and d) parallel configuration with an equivalent SPC capacitance of $2C$ when D_1 and D_3 are conducting. e) Harvesting cycle in the Q - V plane. f) Voltage gain of a SPC-DEG system as a function of the number of cycles.

capacitance of the SPC of $C_{eq} = C/2$ (Figure 8b). Finally, when diodes D_1 and D_3 conduct, the circuit takes a parallel configuration, with an equivalent capacitance of $C_{eq} = 2C$ (Figure 8d). Figure 8e represents the harvesting cycle for a DEG which is deformed until its capacitance is multiplied by 4 (from C_{min} to $C_{max} = 4C_{min}$, i.e., $\beta_{max} = 4$). Initially, all capacitors are discharged. An external low voltage source (not shown in the figure) is briefly connected in parallel with the SPC and the undeformed DEG. This charges both the DEG and SPC (in series configuration) up to a voltage V_0 , at which point the external source is disconnected from the circuit. The DEG starts stretching, and its voltage decreases. At that point, all three diodes are reverse biased, and no charge flow is possible. The SPC is therefore in open-circuit configuration, and the charge on the DEG remains constant, as illustrated by segment (A). However, once the capacitance of the DEG has doubled and the voltage has decreased by a factor 2 to $V_0/2$, diodes D_1 and D_3 become forward biased, switching the SPC to its parallel configuration. The voltage continues to decrease, but charges are transferred from

the SPC to the DEG, as shown by segment (B). As for the triangular circuit of Section 3.1.2, the slope of segment (B) is $-1/C_{eq} = -1/(2C)$. Once the DEG has reached its maximal deformation and starts to relax, the SPC switches again to its open-circuit configuration, and the charge on the DEG remains constant. The voltage increases because the capacitance decreases, as depicted by segment (C). Once the voltage of the DEG doubles, diode D_1 becomes forward biased and the SPC takes its series configuration. Charges are transferred from the DEG to the SPC (segment (D)). Similar to segment (B), the slope of the segment is $-1/C_{eq}$, but as the circuit is in a series configuration, the equivalent capacitance is 4 times lower, and the slope is therefore 4 times larger, which causes the cycle to end up at voltage $V_1 = \alpha V_0$, with α being the voltage gain per cycle. The lighter shade of blue in Figure 8e shows the following cycles. The second cycle ends at $V_2 = \alpha V_1 = \alpha^2 V_0$, and after n cycles, the voltage on the DEG reaches $\alpha^n V_0$. The evolution of the voltage as a function of the number of cycles is shown in Figure 8f. Once a target voltage is reached, the charges can be transferred to a harvesting circuit. As long as some charges are left on the DEG/SPC, it will be able to continue boosting without requiring an external supply. One of the operating parameters of the circuit is the voltage at which the charges are transferred out of the DEG to an external storage circuit. The harvested electrical energy is higher if the DEG is left to work until a high voltage is reached, but the electric BD field puts a practical limit to how high the voltage can be left to build-up before the charges are transferred. In addition to the SPC implementation shown in Figure 8, variations of the SPC have been reported in the literature.^[100,101]

As described earlier, a first-order SPC will switch configuration between its different states when the voltage changes by a factor of two. This requires the DEG to deform enough to provide an increase in capacitance by a factor of two or more, which can be too much depending on the topology of the DEG, and the amplitude of the deformation. However, the concept of the first-order SPC can be generalized to higher orders by paralleling the single unit, at the cost of a larger number of components (Figure 9).^[102] For example, McKay et al. demonstrated voltage boosting using a second-order SPC with a cone DEG, and showed a voltage increase from 10 to 3250 V in 236 cycles.^[64]

Illenberger et al. analyzed the cycle of the SPC in details for a general n th-order circuit.^[102] They showed that the voltage gain α after one cycle is given by

$$\alpha = \frac{(n^2 + n)(C_{min} + C)(\beta_{max} C_{min} + C)}{[n\beta_{max} C_{min} + C(n + 1)][C_{min}(n + 1) + nC]} \quad (10)$$

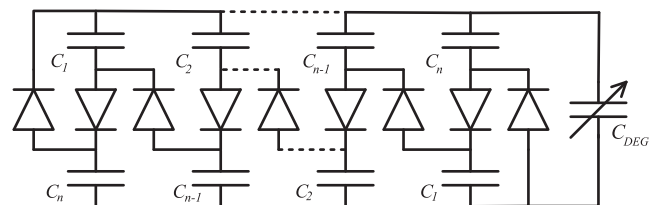


Figure 9. Schematic of an n th-order SPC. The circuit is parametrized in terms of its largest capacitance C , with each capacitor having a value $C_i = C/i$, with i between 1 and n .

with n as the order of the SPC, C_{\min} as the capacitance of the DEG in its relaxed state, C the capacitance of the SPC capacitor, and β_{\max} the maximal capacitance swing of the DEG. At any point of the cycle, the capacitance of the DEG is described by: $C_{\text{DEG}}(t) = \beta(t)C_{\min}$, and $\beta(t)$ between 1 and β_{\max} . As shown in Equation (10), the voltage gain does not depend on the profile of $\beta(t)$ (e.g., sinusoidal, triangle, etc.), but only on its peak value. It can be shown that the voltage gain can be maximized if the capacitance C of the SPC is chosen equal to^[102]

$$C = C_{\min} \sqrt{\beta_{\max}} \quad (11)$$

It is then possible to calculate the gain per cycle as a function of β_{\max} for different orders of SPCs (Figure 10). Depending on the deformation amplitude, there is an optimal order of SPC that should be used to maximize the voltage gain α . For DEGs that have a constant peak deformation, choosing a SPC order is easy. If the amplitude can vary between cycles, and possibly cross the boundary between optimal orders, a choice should be made based on the range of expected amplitudes. For example, if the deformation of a DEG does not ensure a doubling of the initial capacitance, first-order SPCs should be avoided. However, if large deformations leading to an increase in capacitance by at least a factor of three can be guaranteed, then a first-order SPC is the best choice, leading to the largest voltage gain with the simplest circuit topology.

The dependence of the SPC optimal capacitance on β_{\max} (c.f. Equation (11)) appears as a potential issue for the SPC to adapt to varying deformation amplitudes. However, the influence of the value of the SPC capacitance on the voltage gain is limited. Figure 10 shows, with a dashed line, the voltage gain of a first order SPC using a constant SPC capacitance of $C = 1.7C_{\min}$ (i.e., the optimal capacitance for $\beta_{\max} = 3$). As can be seen, there is no visible difference for capacitance swings between 2 and 4, and therefore, a SPC optimized for a defined capacitance swing,

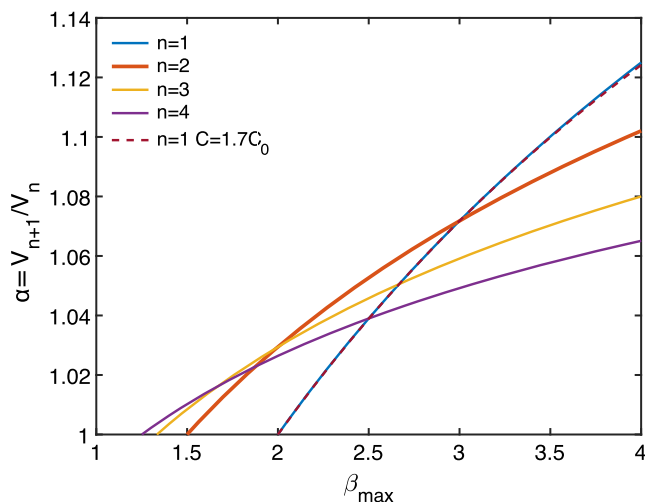


Figure 10. Voltage gain per cycle of a SPC as a function of maximal capacitance swing β_{\max} for circuits of order 1–4. The curves are calculated at the optimal SPC capacitance, except for the last one that uses a fixed capacitance for a first-order circuit.

will still provide close-to-optimal voltage gains if the amplitude does not remain constant.

The voltage gain (Equation (10)) is obtained assuming that the DEG is position-controlled, but force-controlled cycles might be more representative of a real-world application. When the cycle is controlled by an external force of defined amplitude, the deformation amplitude (and therefore capacitance swing) will change as the DEG progressively charges due to the contribution of the electrostatic force induced by the charges. Zanini et al. have modeled a DEG connected to a SPC and subject to a periodic force input, and shown that the system eventually reaches steady-state without further increase in the voltage (i.e., the voltage gain per cycle decreases gradually to 1).^[103] They suggest that this behavior can be used advantageously to design a DEG whose output will saturate below the dielectric BD threshold.

3.2.2. The Integrated SPC

In a further development of the SPC, McKay et al. has integrated the capacitances of the SPC on the dielectric membrane of the DEG to make an integrated self-priming circuit (I-SPC).^[104] The principle of a first-order I-SPC is shown in Figure 11. It consists of two SPC blocks (c.f. Figure 8), realized on the deformable elastomeric membrane itself. The capacitances are therefore stretch dependent. There is not a separate priming circuit and a DEG, but the two elements are combined into a single symmetrical circuit integrated on the elastomeric membrane, and which plays the double role of charge supply and voltage booster. The capacitors of the two blocks must behave antagonistically, i.e., when the capacitors of one block increase their capacitance, the capacitances of the second block must decrease in value. One possible implementation, shown in Figure 11b, is a variation of the pure-shear topology (Figure 2b) comprising a membrane with fixed edges on the left and right, and a slider across the middle of the membrane which is moved sideways. The capacitance values in the two blocks are in phase opposition, and charges are exchanged between blocks to boost the energy of the system. The capacitance of each capacitor is defined as $C(t) = \beta(t)C_{\min}$, and $\beta_{\max} = C_{\max}/C_{\min}$. Similar to the SPC, a first-order I-SPC requires a change of capacitance $\beta_{\max} > 2$, but higher order I-SPCs can be used for DEGs that do not reach such a deformation.^[105]

McKay et al. designed an antagonistic double cone generator, on which four capacitors were patterned (2 on each cone), thus implementing a first-order I-SPC.^[104] They boosted an initial voltage of 10 V to 2 kV in 14 cycles. One of the advantages of the I-SPC over the SPC is that there is a voltage boost each time one of the circuit sides reaches its minimal capacitance, which occurs twice per mechanical oscillation. Therefore, the frequency of the electrical cycle is twice that of the mechanical oscillation, thus providing faster voltage boosting.

Illenberger et al. have modelled the behavior of an n th-order integrated circuit, and have shown that the voltage boost α for each mechanical cycle is given by^[105]

$$\alpha = \left(\frac{(1 + \beta_{\max})(n^2 + n)}{\beta_{\max}n^2 + (n + 1)^2} \right)^2 \quad (12)$$

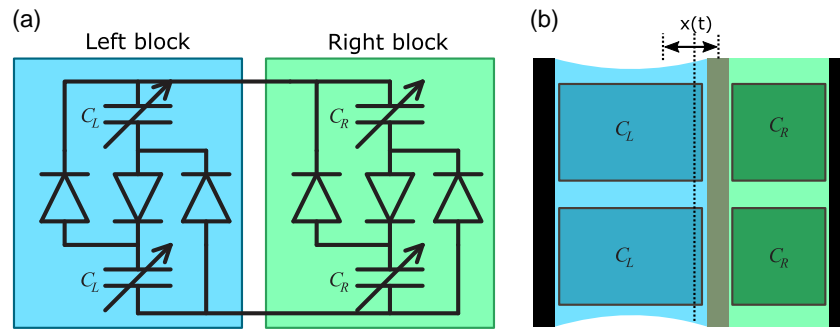


Figure 11. a) A first-order I-SPC. b) Schematics representation of the implementation of the I-SPC in a pure-shear antagonist configuration. The two sides of the membrane are fixed, and the central slider is moved horizontally. When it moves to the left, capacitances C_R increase, whereas capacitances C_L decrease.

with β_{max} as the capacitance swing at maximal deformation and n as the order of the SPC. The power of two stems from the two electrical cycles for each mechanical oscillation of the DEG.

Figure 12 shows the voltage gain per mechanical cycle as a function of the maximal capacitance swing β_{max} , and for different orders of the I-SPC circuit. Similar to the SPC circuit, the optimal order to use for maximal voltage gain depends on β_{max} , and each circuit order has a minimal value of β_{max} below which no voltage boost occurs. These values are identical for the SPC and I-SPC, but the latter provides a higher voltage gain per cycle. For comparison, the voltage gain per cycle of a first-order SPC is also indicated on the figure (dashed line). For example, taking a DEG which is mechanically stretched to provide a maximal capacitance swing of 3, it will take 76 cycles to multiply the initial voltage by 200 if a SPC configuration is used, and 20 cycles with an I-SPC configuration.

Because they require antagonistic motion, I-SPCs are less straightforward to implement. However, some topologies can be easily adapted to bidirectional motion, such as the cone

DEG,^[64,104,106] or the pure-shear DEG (Figure 11b).^[105] In addition to a higher voltage gain per cycle, I-SPC configurations present the advantage of providing more capacitance swing compared with SPC for the same mechanical deformation. Assuming pure-shear deformation ($\beta_{max} \propto \lambda_{max}^2$), the I-SPC configuration of Figure 11b provides $\beta_{max} = 4$ for a displacement of $\pm L/6$ from the central position, with L being the total length of the membrane (left plus right blocks). An SPC configuration would be similar to Figure 2b, for which the same deformation amplitude of $L/3$ would only provide a β_{max} of $(4/3)^2 = 1.78$.

I-SPCs do not require external capacitors, as the entire circuit is integrated on the deformable structure. Diodes are still necessary, but they are small components that can easily be integrated on the frames of the device. DEGs in I-SPC configuration can therefore be made independent from external circuitry. In an effort to show that a completely soft DEG is possible, I-SPC configurations have been developed, in which the hard diodes have been replaced by soft stretch-sensitive switches integrated to the stretchable membrane.^[106,107]

3.2.3. Priming Sources

The SPCs discussed earlier require an one-time input of energy to start. If they stop moving, charge leakage will slowly decrease the amount of charges on the device, and if the period of inactivity is long enough to completely deplete the charges, they will not be able to start again. Sources of priming charges enable to make DEGSS truly independent from an external power source, thus making small-sized DEGs interesting candidates for distributed applications such as power source for wireless sensor networks or wearable applications.

Jean-Mistral et al. introduced the combination of permanently charged dielectrics (electrets) with soft energy harvesters.^[108] They proposed two different configurations (**Figure 13**): the dielectric mode in which the electret is used as a polarizing source, and the electret mode, which is similar to the standard electret generator configuration used to scavenge vibrations, but taking advantage of the compliance of the elastomer to develop wearable applications.^[80,108]

The dielectric mode is similar to the harvesting cycle obtained with the triangular circuitry (c.f. Section 3.1.1), with the same

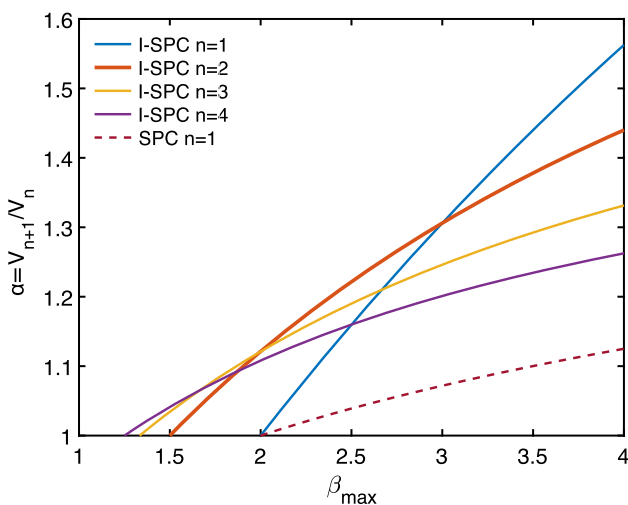


Figure 12. Gain of an I-SPC per mechanical cycle as a function of the maximal capacitance swing β_{max} for circuits of orders 1–4. As a comparison, the gain obtained for a first-order SPC circuit is also given.

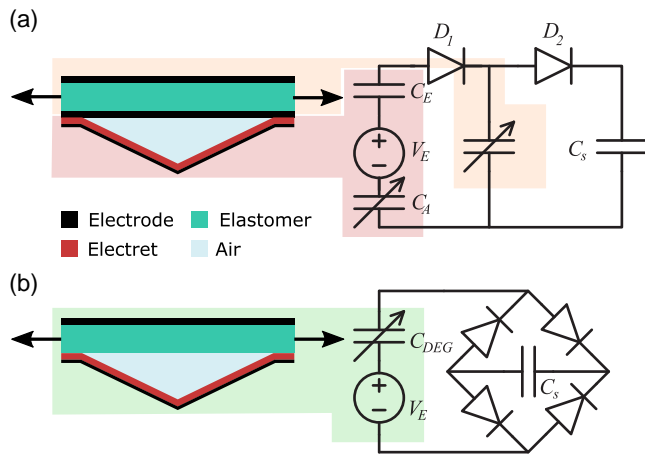


Figure 13. a) Electret used in the dielectric mode. when the DEG is stretched, the V-shaped electret^[80] is flattened, leading to an increase in the air gap capacitance C_A , reducing the voltage drop across it. When the electret gets close to the membrane, its voltage V_E is split between the DEG capacitance C_{DEG} and the electret capacitance C_E . b) Electret mode: in this case, the electret is integrated on the variable soft capacitors, and current fluctuations of opposite directions are created each time the air gap closes and opens. A rectifier bridge with four diodes can be used to accumulate the charges generated by these fluctuations into a storage capacitor.^[80]

consideration on the value of C_s . However, instead of an external power source, the priming charges are provided by an electret whose distance from the DEG varies during the cycle^[80,108] (Figure 13a). When the DEG is fully stretched, the V-shaped electret is fully flattened against the DEG, and therefore the capacitance of the air gap C_A is maximized, thus dividing the electret voltage V_E between C_{DEG} and C_E . A diode (D_1) is connected between the top electrode of the DEG and the bottom electrode of the electret capacitor, to prevent the charges to flow back to the source when the DEG is relaxed. The voltage of the DEG increases and its charges can transfer to the storage capacitor C_s . Teflon charged with a negative potential retains its charge for months and can be used as a priming electret.^[80] Because electrets are not stretchable, harvesters must be designed to accommodate them, e.g., by including a V-shape structure,^[80] or taking advantage of the fringing electric field to place the electret and DEG side by side.^[109]

The electret mode (Figure 13b) integrates the electret and the stretchable capacitor into a single electret harvester, which generates a current fluctuation of opposite sign each time the air gap opens and closes.^[80,110] A rectifier bridge can then be used to collect these charges into a storage capacitor.^[80]

In a variation of the circuit of Figure 13a, Illenberger et al. implemented an electret with an I-SPC (c.f. Section 3.2.2), thus combining the double advantage of the electret as a source of priming charges, with the voltage-boosting capabilities of the I-SPC.^[111] In their configuration, the electret provided a biasing voltage of 200 V, and they compared the performance of the I-SPC with a CC cycle (c.f. Figure 7 and Section 3.1.2). The latter produces a constant amount of electrical energy per cycle, whereas the energy generated from an I-SPC increases with the number of cycles. They showed that the amount of energy

per cycle obtained from an I-SPC exceeds that of the CC circuit after 10 cycles. Therefore, if the charges from the I-SPC circuit are harvested after a sufficient number of cycles, the amount of collected energy will be higher than with the CC circuit.^[111] The choice between using a CC circuit or an I-SPC therefore depends on the application: if the source of mechanical energy is irregular, with possible periods of inactivity between cycles, then the CC circuit should be used, as it will output energy at each cycle, whereas inevitable leakage would cause the charges of an I-SPC to be depleted after a period of inactivity. However, if the source of mechanical input is regular enough to provide a few uninterrupted cycles, then the I-SPC will provide more output energy.

Piezoelectric materials can be used instead of electrets as a source of priming charges, with similar configurations and circuits. The use of piezoelectric materials, namely lead zirconate titanate (PZT) diaphragms and polyvinylidene fluoride (PVDF) films, have been demonstrated as a source of priming charges for DEGs.^[112–114] The proposed designs include a mechanism that applies stress to the piezoelectric material when the DEG is in its stretched state, to generate charges that are then transferred onto the DEG. Piezoelectric materials on their own are used to convert mechanical energy into electrical energy (piezoelectric energy harvesters^[115]), but a hybrid generator combines the ability of the piezoelectric material to generate electrical charges with the ability of the DEG to increase the electrical potential of these charges. Mathew et al. have presented a piezoelectric–DEG hybrid generator using a triangular harvesting cycle (c.f. Section 3.1.2) that produces an electric energy density 80% higher than that produced by the PZT alone.^[113] In a further improvement, they replaced the harvesting circuit with a first-order SPC (c.f. Section 3.2.1) and obtained a specific energy output 19 times higher than the PZT working alone.^[114]

The combination of a source of priming charges (electret or piezoelectric material), a DEG, and an SPC, makes it possible to fabricate compact systems that are completely independent from an external supply. These systems are able to generate specific energy on the order of a few mJ g^{-1} . Despite being only a fraction of the maximal energy density that a DEG can harvest, this topology is particularly interesting for wearable or distributed applications, for which the required power is low, but which need to operate without external electrical supply.

3.2.4. High-Voltage Stepdown for Portable and Wearable Applications

Harvested high-voltage charge on the elastomer must be stepped down by up to 3 orders of magnitude to be useful for powering small portable or wearable electronic devices. In what is perhaps the first study to efficiently convert DEG voltage (low-to-high for charging and high-to-low for discharging), Due et al. used a boost/buck converter circuit.^[116] While they reported high efficiency of 90% for a 1 order of magnitude drop from 2 kV to 300 V, their circuit required active high voltage switches, sensors, and diodes. They did not report on the energy costs associated with the active elements. Several strategies for voltage conversion have been explored by Eitzen et al.^[117] The topologies investigated included bidirectional flyback converters. In another study, the same authors showed that by stacking of multiple converters

in series on the stepdown side, a large voltage conversion could be achieved without the need for high-voltage switches.^[118] They also demonstrated the feasibility of an experimental bidirectional flyback converter that did not include a DEG. Panigrahi et al. used a flyback transformer circuit for voltage stepdown of a small DEG alongside a form of SPC.^[119] While the overall global efficiency was less than 1%, they reported good efficiency for the stepdown of 79%. However, they did not report on the associated energy costs of the circuit. The energy costs of using active electronics, that includes sensors and controllers will grow in relative significance as the DEG reduces in size. DEGS that are wearable will be small in volume, on the order of 1 cm^{-3} . From such small generators, the expected power output operating at frequencies around 1 Hz (e.g., for human energy-harvesting applications) will be on the order of milliwatts.^[26] Squandering such power on active controllers and sensors is very likely to be unaffordable and could cost more than the energy harvested. Therefore a key goal for small wearable DEGS is to obtain efficient and substantial voltage stepdown without the need for external power for switch and sensor control. One strategy is to do this passively, triggered solely and synchronously with voltage changes across the capacitance of the DEG, thus obviating the need for externally powered sensors and switches. With this goal, Lo developed a self-powered converter that used as a packet of DEG overflow energy from a breakover circuit to drive a fast switching metal-oxide-semiconductor field-effect transistor buck converter.^[120] This was a fully passive circuit, controlled by the DEG itself. This circuit was able to achieve 43% energy extraction from a DEG in an almost 2 order of magnitude stepdown from 914 to 5 V. Another approach involved passively switching a flyback converter above a threshold voltage from the DEG.^[121] Any one of a number of passive switch devices could be applied to this including, spark gaps, thyristors, avalanche diodes, breakover diodes, discharge tubes, and thyristors operated as breakover diodes. A circuit based on this principle was investigated by Ikegame and Takagi.^[122] This work was preceded by their investigation of a Zener diode to step the voltage down to a capacitor, with less than 1% efficiency.^[123] Using the flyback converter idea they showed that high efficiency is possible (order of 70%) with an adequate stepdown transformer.

As it stands, voltage stepdown for wearable and portable DEGS is both feasible and efficient and given its recent appearance on the scene will be open to further discovery.

3.3. High-Power Electronics

While off-the-grid-independent operation is a requirement for low-power-distributed applications, constant power input is not an issue for large-scale energy-harvesting installations, which are meant to be connected to the network. Instead, the priority lies with the maximization of the generated power, and the minimization of losses. In this context, the harvesting cycles requiring electrical energy input W_{in} for each cycle are interesting candidates, as they enable to harvest more energy per cycle. But beyond this value, the ratio of net energy gain versus energy input required for each cycle is another important metric (Table 3, column 4). As real-world systems must be designed with reliability and lifetime in mind, they cannot operate

anywhere close to the limit of MR of the material. Furthermore, the amount of deformation of the DEG will be limited by the physical implementation (c.f. Section 4), and leads to low values of β_{max} . Consequently, the ratio of net energy gain versus the energy input can be lower than 1^[124] (Figure 7f), leading to a required power rating for the driving circuit significantly higher than the average output power, and to an important impact of the losses on the conversion efficiency.^[125] High-power DEGS-based-harvesting systems require efficient electronics to manage the input and output of electrical energy. They must provide bidirectional energy flow, be suitable for a variable output voltage and current caused by the variable capacitive load, and be adapted to the high-voltage levels required to operate DEGSs at maximal efficiency.^[124]

Eitzen et al. have proposed a bidirectional flyback converter design for DEG applications that addresses the needs mentioned earlier.^[124] Their concept relies on the cascading of identical modules, each with a power rating of about 200 W. The modules have their primary sides connected in parallel, and secondary sides in series. This input-parallel output-series (IPOS) cascading enables to reach the high driving voltages required by DEGS while using standard electronic components. They have designed a plant to control the switches of the converter to operate in boundary conduction mode, as this is the most efficient for capacitive loads. The controller also limits the current on the secondary side, so as not to damage the electrodes of the DEG.

Another high-power configuration is the dual active bridge (DAB).^[125–127] Similar to the flyback configuration mentioned above, a IPOS cascading approach can be used,^[125] or a single primary stage with several secondary sides connected in series.^[127] For example, Todorovic et al. have developed a IPOS DAB-based bidirectional converter with an average output power of 5 kW for wave energy conversion. To improve efficiency and provide a large operating power range, they investigated three different modulation schemes for the DAB. While two different trapezoid modulations were able to cover specific zones of the current-voltage state space at higher efficiency, a triangular modulation was able to cover the complete output power range in terms of voltage and current, but at the cost of higher losses. The authors then proposed an hybrid modulation scheme, selecting the most efficient modulation on the fly depending on the output current and voltage at any time. In the context of wave energy conversion, they calculated the expected ratio of effective electrical energy output over available harvestable energy for incoming waves of different amplitudes and frequencies, and obtained an average value of 66% with the hybrid modulation, which is 13 percentage point higher than using the triangle modulation mode alone.^[125]

These high-power circuits enable to precisely control the voltage on the DEG, and therefore, make it possible to implement any energy-harvesting cycle. In particular, they can implement a CE cycle, which leads to the highest possible energy gain per cycle,^[124,128] and which is not achievable with the circuits presented in Section 3.1 and 3.2. Because of the large number of components they require and the need for precise feedback control, these circuits are well suited for large-scale harvesting applications, for which a high conversion efficiency is paramount.

4. Prototypes and Applications

4.1. Proofs of Concept for Energy Conversion Optimization

This section presents an overview of theoretical and experimental works aimed at assessing the maximum practical convertible energy of DEG units, regardless of their final applications.

The convertible energy density achievable with practical DE materials can be roughly estimated based on the analyses drawn in Section 2.4 and the data in Section 2.5. Based on Table 2, assuming a permittivity ϵ of 2–4 times the vacuum permittivity, BD strength E_{BD} in the range 50–150 MV m⁻¹ (higher experimental values have been also reported at large applied stretches),^[18,61] the theoretical convertible energy density is in the range 0.06–2.5 J cm⁻³ (i.e., 0.06–2.5 J g⁻¹, as elastomers density is close to 1 g cm⁻³) assuming a maximum-to-minimum stretch ratio in the range 2–5 and equibiaxial deformation (see Equation (5) and Table 1). This is at least three orders of magnitude more than the energy density of piezoelectric harvesters^[129,130] and 10–100 times more than electrostrictive polymers,^[131] which exploit significantly smaller strains.

Theoretical estimates are available in literature that rely on an accurate computation of the maximum convertible energy of a DEG through the identification of its feasible working space (as shown in Figure 4). Compared with the rough estimate presented earlier, those works consider: 1) the feasible stretch range based on MR and EMI limits, 2) experimental relationships for the BD strength as a function of the applied stretch (namely, E_{BD} has been reported to increase with the applied surface stretch).^[31] With reference to equibiaxial deformations, Koh et al.^[31] and Jean-Mistral et al.^[132] reported achievable energy densities of 1.7 and 3.2 J g⁻¹, respectively for a reference acrylic elastomer. Considering natural rubber DEs, Koh et al.^[31] estimated convertible energy densities on the order of 1.3 J g⁻¹, whereas Kaltseis et al.^[18] predicted the densities of 3–3.5 J g⁻¹ by assuming to further push the materials limits in terms of stretch and electric field. Compared with rubber, acrylic elastomers provide larger maximum stretch and have larger permittivity. However, they typically feature a lower BD strength^[61] and, due to their low elastic modulus, suffer the limitations of EMI.

Following up to theoretical estimates on DEG convertible energy density, dedicated experimental research has been conducted to push DEGs performance to the limit. State-of-the-art

experimental values of the convertible energy density are on the order of a few hundreds of mJ g⁻¹.^[18,19,33,35,46,48] The differences with respect to theoretical predictions are due to: 1) the effect of losses discussed in Section 2.4;^[41] 2) practical control loops (Section 3.1), that do not pursue a perfect tracking of the maximum-energy cycle (Figure 4), hence providing suboptimal performance.

An overview of the experimental peak energy density performance obtained with different DEG topologies and DE materials is shown in Table 4. Up until now, acrylic VHB has largely been the most used material for demonstrators, and the largest converted energy density has been achieved using this material.

Recent tests with pure-shear and conical DEG samples led to densities of 190 and 130 mJ g⁻¹, respectively.^[35,42] Although the conical and pure-shear topologies provide similar deformation kinematics and surface stretch ratios, the density obtained by Song et al. with pure shear is larger, as a result of larger applied electric fields,^[35] in spite of large strains used by Jiang et al. in cone DEG demonstrators.^[42] In both tests, an OT control cycle (Section 3.1.2) was used, so as to efficiently fit the DEG maximum-energy cycle (Section 2.4).

Previously, Kaltseis et al. had reached densities of 102 mJ g⁻¹ (with power density of 17 mW g⁻¹ and efficiency of 7.5%) using an acrylic inflatable DEG diaphragm.^[46] Compared with other works, they set up electronics able to deliver the generated energy to a storage utility (instead of dissipating it on resistive probing loads) and pursued a direct measurement of the generated energy, rather than estimating it from the measured DEG output current and voltage. To do so, they used a CCCV control loop (Section 3.1.1) which covered a limited area of the DEG's feasible workspace, hence allowing the conversion of a limited amount of energy per cycle.

Consistently with theoretical predictions, the largest energy density was demonstrated in equibiaxial loading conditions.^[19,33] In a first work, Huang et al. achieved energy densities of up to 560 mJ g⁻¹, power densities of 280 mW g⁻¹ and mechanical-to-electrical conversion efficiency of 27%.^[33] Then, Shian et al. hit the remarkable target of 780 mJ g⁻¹ converted energy density by resorting to an OT loop.^[19] This figure, which represents the largest density scavenged to date with a DEG, was obtained using maximum electric fields close to the material BD limit.

Despite its suitability to achieve remarkable conversion performance on a single-test basis, VHB is considered scarcely reliable

Table 4. Experimental convertible energy density performance obtained with different DEG prototypes.

	Ref.	Topology	Control cycle	Max electric field ^{a)} [kV mm ⁻¹]	Max stretch ^{a)}	Energy dens. [J g ⁻¹]
Acrylic (VHB 4905/4910)	[35]	Pure shear	OT	100	5	0.19
	[42]	Cone	OT	75–80	7.5–8	0.13
	[46]	Circ. diaphr.	CCCV	85–100	5–5.5	0.10
	[33]	Equibiax.	CCCV	170–180	5.4	0.56
	[19]	Equibiax.	OT	180	5.5	0.78
Natural rubber (OppoBand 8003)	[18]	Circ. diaphr.	CCCV	150–170	4.5–5	0.37
Silicone (Elastosil 2030)	[65]	Circ. diaphr.	OT	110–150	2.5–3	0.17

^{a)}Estimated from the data in the references.

for applications which are required to last in time. Attention has been thus recently moved also on other DE materials.

Using a tougher commercial natural rubber elastomer, Kaltseis et al.^[18,46] obtained a convertible energy density of over 3 times that achieved with VHB acrylic using a highly stretched inflated circular diaphragm DEG (so as to produce nearly equibiaxial deformations) and a CCCV control loop. They obtained densities of 369 mJ g^{-1} (200 mW g^{-1}) and 7.2% efficiency, with peaks of 15% in other tests), hence proving the potential of natural rubber for energy-harvesting applications.

Moretti et al.^[65] performed energy harvesting tests on a silicone circular diaphragm inflating DEG. They used power electronics and a harvesting cycle similar to those proposed by Shian et al.^[19] but they used lower maximum stretch than Kaltseis et al.^[46] They achieved maximum energy density of 173 mJ g^{-1} , power density of 86 mW g^{-1} . Thanks to the reduced mechanical loss of the silicone elastomer, they achieved efficiencies of up to 30% compared to acrylics and rubbers. Though, to date, silicone DEs have been scarcely used in energy-harvesting applications, a significant boost in research is expected to occur in the next few years by recent advances in material science, which are delivering silicone elastomers with largely improved electromechanical properties.^[60,66]

4.2. Energy Harvesting from Human Motion

Wearable technology includes communication devices (e.g., headphones, microphones), powered prostheses, exercise monitors, and a growing plethora of sensors for physiological monitoring.^[133] Many can operate at the mW level, although powered prostheses and other devices for locomotor system augmentation and therapy have power requirements on order of 1 W and require frequent recharging.^[134] The food we eat, with tens of times the energy density of batteries, enables us to meet our own running costs that are roughly equivalent to the energy stored in hundreds of AA batteries per day.^[134] Diverting some of this power to running or recharging of wearable devices is compelling. However most of this metabolic energy is lost in heat and any attempt to harvest thermal energy will be limited by an inherent low Carnot efficiency and the practical issues associated with large surface area coverage of a human body. Fortunately, we also expend substantial energy when we walk and run.

At a walking frequency of 1 Hz, a maximum power of $\approx 4 \text{ W}$ is obtainable.^[134] This can be verified using a simple calculation. As we decelerate our body, loading of the heel can exceed one body weight; and generate forces on the order of a kN. If during this time our heel deflects by 4 mm, say, we are doing work on the heel of about 4 J per heel strike. However, a large fraction of the strain in the shoe heel is elastic; thankfully so, for if we were to harvest all the energy in the heel we would have the experience of walking on sand. Realistically, we want to harvest the energy that would normally be lost due to the viscoelasticity in the heel material. There are further opportunities for energy harvesting from human motion using DEGs, particularly from the rotation of the lower limbs including the ankle joint, hip, and knee for which muscle power is order of tens of watts during walking with much of the power expended during braking.^[134] Thus, we have an opportunity to assist the body and perhaps even return power

to storage synonymous with automotive regenerative braking systems.

Perhaps, in the earliest demonstration of DEG locomotor system energy harvesting, Kornbluh et al. described a heel strike generator in a boot that could harvest 0.8 J per cycle of walking.^[135] Heel compression resulted in pneumatic stretching of DE diaphragms in an array (Figure 14a).

Effort associated with DEG human energy harvesting has involved specific aspects of performance enhancement that are beneficial for portable and also wearable uses, rather than full demonstrations on the human. Lai and Read showed, through a modeling study, how a stretched DEG incorporated into a knee sleeve brace could be used for modifications to gait for the patient.^[137] Jean-Mistral et al. developed an experimental mechanism that could harvest energy from the moving human knee.^[138] The device that was to be located behind the knee supported a stretched VHB membrane. They projected that with a high bias voltage of 1 kV they could harvest 1.74 mW; a value of

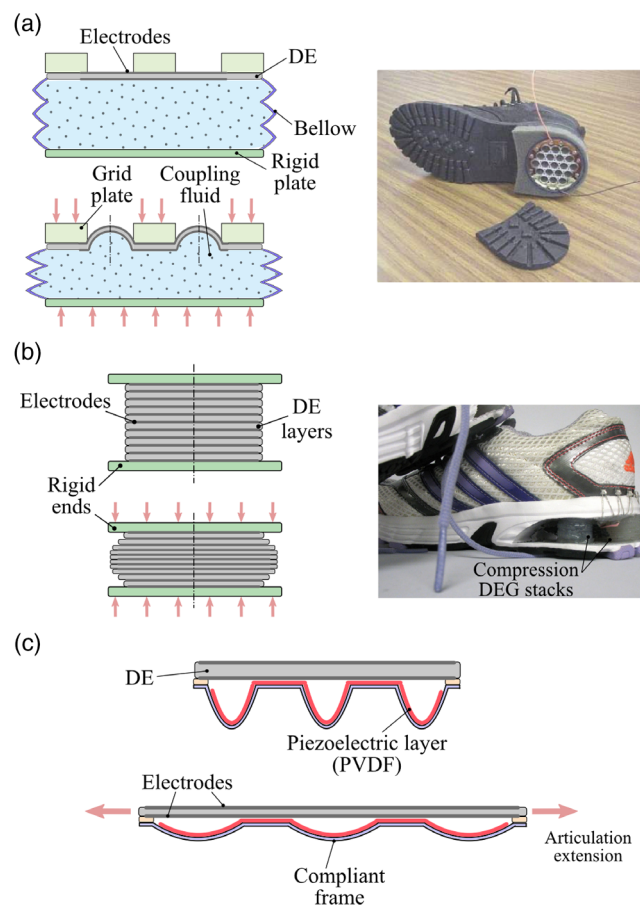


Figure 14. Human motion energy harvesting with DEGs. a) Schematic and picture of the heel-strike energy harvester based on inflatable DEG proposed by Kornbluh et al.^[23] b) Schematic and picture of the heel-strike energy harvester based on compression DEG stacks proposed by the University of Auckland.^[136] c) Layout of a DEG with piezoelectric priming source for energy harvesting from knee articulation, as proposed by Lagomarsini et al.^[112] (a) Reproduced with permission.^[23] Copyright 2012, Springer Nature.

power that is adequate for small electronics. Jean-Mistral and Basrouir have developed a tubular DEG as a demonstration step for integrating this technology with textiles. They produced a demonstrator consisting of silicone tubing 1.9 mm diameter, 100 mm long and with 0.2 mm wall thickness. From their results, they projected that a 300 mm length subjected to strains from the knee at walking speed could generate a milliwatt of power.^[139]

The devices described earlier would rely on direct tensile strain in the membrane. This can be amplified as demonstrated by Mathew et al., who built a fully autonomous compression-activated harvester that can deliver a piezoelectric priming charge to a DE membrane during stride and whose stretch is magnified further by mechanical means.^[114] Their calculated output energy density was 0.49 mJ g^{-1} ; for a 1 g device ($\approx 1 \text{ cm}^3$) we would expect about half a watt at 1 Hz.

An alternative approach is to use direct compression in a multilayer stack (Figure 14b), like the one built by McKay and coworkers, that was order of 1 cm^3 in volume.^[26,34,136] This device could produce milliwatts of power at physiological frequencies. One advantage to the compressive layered design is the prospect of it being substituted directly for the rubber heel itself.

Improvements to electronics portability and wearability have been previously described in Section 3.2. Specifically these are associated with passive circuitry for self-priming,^[64,104,107] the use of electrets for priming,^[80,110] piezoelectric generators for initial charge (Figure 14c),^[112] and passive circuits for voltage stepdown.^[120–123]

In summary, while there have been few, if any, published examples of human energy harvesting using DE generators, the technology to enable wearable and useful DE harvesting does exist. And with a little more effort, it should be possible to put a DE generator unobtrusively in a person's shoe or on their shirt.

4.3. Energy Harvesting from Ambient Sources and Renewable Energy

Traditional machinery for power generation (either from fossil fuels or ambient energy sources) relies on layouts that are optimized for specific operating conditions (frequency, type of motion, and scale), but are not flexible in terms of scalability and adaptability to applications that are other than those they were designed for.

In contrast to that, DEGs bear features that make them particularly promising in applications where conventional machines would struggle or offer poor flexibility.^[140] Application of DEGs in a diversity of energy harvesting scenarios has been envisaged, driven by the following considerations: 1) In contrast with thermal or electromagnetic machines, DEGs feature drastically simpler layouts, which rely on cheap materials and few (or no) rigid moving parts. Among other, this offers a strong motivation for DEGS application in renewable energy harvesting (Figure 15a,b),^[141] where low capital costs are key to economic feasibility. Furthermore, the perspective of delivering generators free from moving parts (but the polymeric membranes) led to consider DEGs applicability in thermal systems such as fully polymeric combustion engines (Figure 15c).^[23] 2) The DEGs' response naturally complies with the features of some ambient sources. For example, DEGs are particularly suited to handle alternate linear motion and operate at low frequencies or low speeds with no need for mechanical transmissions, as opposed to electromagnetic generators.^[140] This has triggered research in ocean wave energy,^[23,141,142] where generators capable to efficiently operate at 0.05–0.2 Hz driven by the waves oscillations are required. 3) The DEG principle and layouts are suited for implementations at different scales, from milliwatt-scale applications possibly up to kilowatts/megawatts. This led to envisage different dimensional targets, i.e.: 1) small-scale systems (10^{-3} to 1 W) to power sensors and electronic equipment via recovery of waste vibrational energy;^[143] 2) intermediate-scale systems (1–1000 W) capable to harvest renewable energy to feed local utilities;^[140] and 3) large-scale systems ($>1000 \text{ W}$) for grid electricity production.^[49]

To date, experimental demonstration of DEGS-based energy scavenging from ambient and renewable energy sources has been provided via scaled laboratory prototypes (up to roughly 10 W of power).^[48,49,140] Several theoretical estimates and numerical simulations have been carried out, which suggest that large-scale energy harvesting from ambient sources (wind and waves) is in principle feasible,^[18,144] with bounds that are only due to current technological restrictions (e.g., manufacturing process and electronics upscaling).

We hereby present an overview of the state-of-the-art of DEG systems and prototypes investigated to date with reference to three applications: 1) vibration energy harvesting; 2) mechanical renewable energy harvesting; and 3) thermal energy harvesting.

Vibration energy harvesting aims to recover mechanical energy (that would be otherwise wasted) from a vibrating source

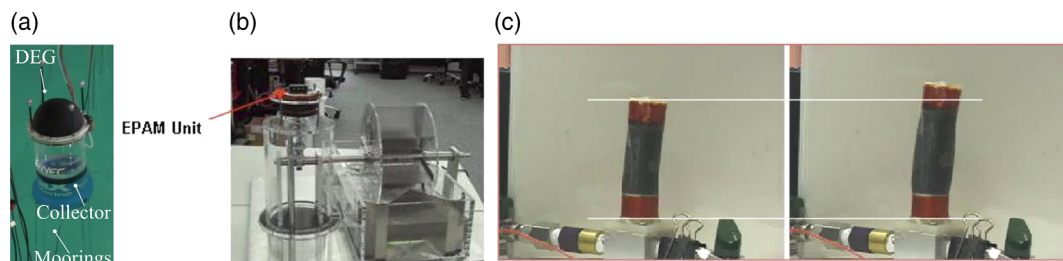


Figure 15. Examples of DEGS prototypes for energy harvesting from ambient sources and renewable energy. a) A prototype of a WEC with circular diaphragm DEG.^[141] b) Laboratory prototype of a water mill generator for currents energy harvesting.^[23] c) Internal combustion engine based on a deformable DEG cylinder.^[23] b,c) Reproduced with permission.^[23] Copyright 2012, Springer Nature.

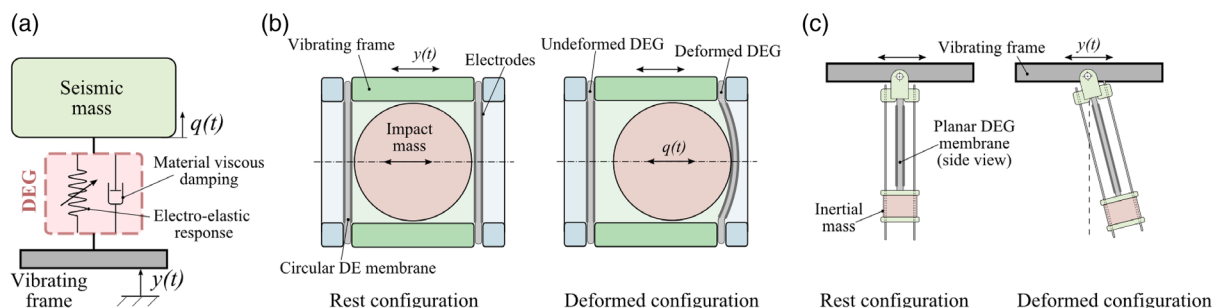


Figure 16. Vibration energy harvesting with DEGs. a) Schematic of the general working principle. b) Impact-mass harvester proposed by Thomson et al.^[143] c) Impression of a DE pendulum harvester, as proposed by Fan et al.^[146]

(a structure or a machine tool) to supply small-power utilities (e.g., distributed sensor). DEGS-based vibration energy harvesting exploits the well-known principle of the inertial energy harvester,^[145] schematically shown in **Figure 16a**. The harvester consists of a seismic mass connected to a vibrating frame (e.g., a structure or the shield of a machine) through a DEG. In the passive state (without voltage), the DEG behaves as a suspension between the vibrating frame and the seismic mass, and is thus cyclically stretched as a result of phase shift between the oscillations in the two components. The suitable control of the voltage on the DEG as a function of its deformation (Section 2.1) provides the system oscillation to be damped and leads to power generation.

Based on this principle, Thomson et al.^[143] proposed a system in which the seismic mass is a ball that can freely oscillate along the axis of a tubular structure, closed at the edges by two flat DEG membranes. Vibrations applied on the system through the tubular frame trigger the mass oscillations and the alternate out-of-plane deformation of the membranes (**Figure 16b**). The authors designed and performed numerical analysis of a milliwatt-scale generator capable to operate at frequencies of 10–50 Hz.

Fan et al.^[146] proposed a DE-based pendulum harvester. The system, schematically shown in **Figure 16c**, consists in a flat DE membrane which has one end attached to a vibrating frame and the other holding the seismic mass, which can freely oscillate in the longitudinal direction (on the membrane surface plane). Relative oscillations between the frame and the mass generate cyclical stretching of the DE membrane. To demonstrate the operating principle of the system and validate analytical models, the authors built a prototype using acrylic VHB as the DE and operated it at low frequencies, achieving convertible power densities on the order of 2 mW cm^{-3} . Consistently with established results in the field of inertial energy harvesting,^[73,145] they pointed out that the system delivers maximum power output when the vibrations excitation frequency equals a natural frequency of the system, i.e., in resonance conditions.

Preliminary works suggest that inertial energy harvesters based on a DEG suspension can perform effectively, provided that their response is tuned with that of the vibrating structures. Nonetheless, the ability of DEGs to efficiently work at high frequencies (e.g., 10–100 Hz, consistent with structural vibrations) is to date loosely proven. Research on material science and the development of low-viscosity DEs seems key for vibration harvesting applications to be successful.

Mechanical renewable energy harvesting via DEGs includes: 1) harvesting from continuous fluid streams (wind or water currents); and 2) harvesting from sea waves.

As regards energy harvesting from fluid streams, it has been observed that DEGs might carve out a niche for themselves in low-power (<1 kW) standalone applications, as opposed to large-scale traditional technologies for grid supply.^[140] This especially applies for water current harvesting, which is still in a landscaping precommercial phase,^[147] whereas in wind energy applications, competing electromagnetic technologies have set a standard even at the smaller scale. In this context, DEG systems might be used to recover energy from water resources which are of no interest for large-scale power production, like river flows or mild tidal currents.^[23,140] Coupling the continuous input mechanical energy from wind and currents with DEGs is however challenging, as the latter naturally pursue a cyclical generation principle. Proposed solutions take advantage either of mechanical transmissions or by structural vortex-induced vibrations.

Chiba et al.^[148] built a first demonstrator of a flow energy harvester using a waterwheel as an intermediate kinetic energy absorber (**Figure 15b**). Relying on a mechanical transmission to drive the DEG deformation, this system does not take full advantage of DEGs features in terms of compactness and architectural simplicity.

Maas and Graf proposed a system which relies on a submerged stretchable DEG pipe to harvest the power of water flows.^[149] The system, schematically shown in **Figure 17a**, consists of a DE tube with electrodes on the inner and outer surfaces. One end of the tube is rigidly connected to the river or sea bed. The other end is free to move longitudinally, and it holds a flange and a shutter to control the end's aperture. When the shutter is open, the pipe is prestretched by the hydrodynamic pressure generated by the flow on the flange. Closing the shutter generates a shock wave which causes a longitudinal stretching of the pipe (forward wave), followed by a contraction (reflected wave from the inlet section). Piloting the shutter openings/closures allows to achieve a cyclic deformation and, hence, to convert mechanical power from the flow into electrical power. The frequency of the oscillation depends on the geometry of the system and the DE material elastic modulus. The authors elaborated a theoretical model of the system and performed in-field mechanical tests on a small-scale prototype to characterize the fluid-structure interaction response. Similarly to the aforementioned

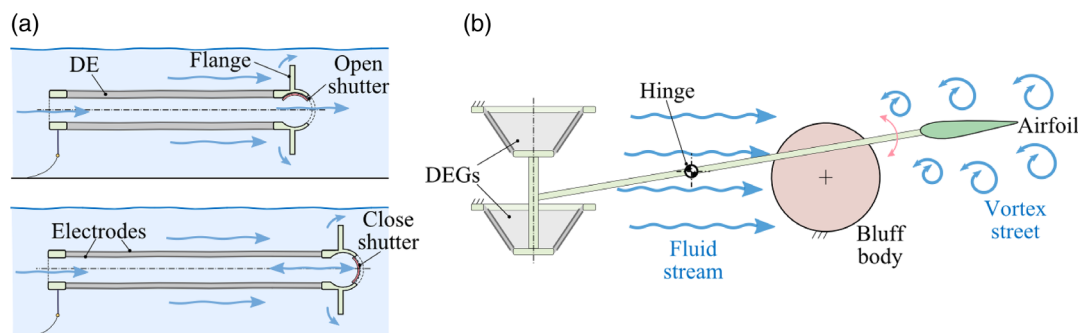


Figure 17. Energy harvesting from fluid streams with DEGs. a) Impression of a stretchable tube water flow generator, as proposed by Mass and Graf.^[149] b) Impression of a generator driven by vortex-induced vibrations, as proposed by Chiba et al.^[150]

conclusions on vibration energy harvesting, they pointed out that the generator theoretically converts maximum power when its natural frequency equals the frequency of the shock waves (namely, at resonance).

Chiba et al. proposed and implemented a system which takes advantage of vortex shedding over a pitching structure to harvest energy from water currents^[150] or wind.^[140] The system (Figure 17b) consists of a bluff body which is responsible for vortex generations, and a hinged structure, put into oscillations by the vortex street, which drags the deformation of one or more DEG units. The authors tested a prototype device in a water channel. Using two-cone DEGs (each bearing 0.1 g of acrylic DE material) as the power take-off (PTO) system, they achieved power outputs on the order of 30 mW at oscillating frequencies of roughly 1.5 Hz (i.e., the natural frequency of the vortex excited system), with current-to-electrical measured conversion efficiency of up to 7.5%.

Vortex-induced vibrations have been later studied by Lai et al.,^[151] who proposed a wind energy generator consisting in a flexible cantilever beam, holding at the edge a bluff body, within which an inertial energy harvester (similar to that shown in Figure 16) is housed.

The mentioned concepts for the exploitation of fluid streams make use of DEGs combined with hydro/aerodynamic interfaces, typically including rigid structural or moving parts. To take full advantage of the DEG features, some authors have envisioned that, in the future, wind or current energy harvesters might be investigated which exploit vortex-induced vibrations over flag-like compliant structures entirely made of DE material.^[23,140]

Opposite to fluid flows, ocean waves have characteristics which intrinsically match the working principle of DEGs (low frequencies and oscillatory behavior).^[23] Currently, wave energy scavenging is one of the most widely investigated DEG applications, therefore, a dedicated review of this topic is shown in Section 4.3.1.

Finally, it has been proposed that DEGs might be used to generate electrical power from thermal energy sources, though this is, to date, a seldom explored topic. Chiba and Waki^[140] suggested that DEGs can be used as the PTO system in concentrated solar power. They proposed a system in which the thermal energy delivered by a concentration system is used to cyclically expand a fluid (or gas volume) and drag a DEG's deformation.

More radically, Kornbluh et al.^[23] suggested that DEGs might be used to build disruptive low-power internal combustion engines, in which the piston-cylinder set is replaced by a tubular deformable structure made of DE. In a pioneer work, the authors claimed that they operated a DEG engine (Figure 15c) at combustion temperature, achieving fuel-to-mechanical conversion efficiency of 11%.

4.3.1. Wave Energy Harvesting

In spite of significant research and development efforts to develop systems capable of capturing the power of sea waves,^[6] wave energy converter (WEC) technologies have not reached technological readiness yet. The limitations for mechanical and electromagnetic technologies to meet the requirements of the marine environment have triggered research toward radically new WEC technologies.^[6] In this context, DEGs have been recognized as a potential game-changing solution^[6,23] Some of the potential advantages of DEGSs, compared with electromagnetic, hydraulic or turbo machinery, are: the architectural simplicity and low costs of the raw materials, which might significantly reduce the capital costs; the low mass density, which would make installation and replacement operations simpler and cheaper; the resilience of DE materials and their resistance to corrosion; and the good matching between low wave frequency and DEGs working cycles.

It has been suggested that DEGS-based WECs might provide an affordable solution for small-power utilities (e.g., navigation buoys^[152]), however, the far most relevant and attractive application in terms of market dimension is large-scale power generation. The wave energy community has recognized that, for wave power plants to be economically viable, WEC units should have rated powers of hundreds of kilowatts and they should be installed in large megawatt-scale farms.^[153] Assuming that DEG PTO systems will be able to provide power densities on the order of $\approx 100 \text{ W kg}^{-1}$ (Section 4.1), single WEC units will require an amount of DE material on the order of tons to reach the envisaged target power.

Compared with this vision, DEGS-based wave energy harvesting is today in a scouting and proof-of-concept phase. Small-scale prototypes and demonstrators have been mainly operated in laboratory environment. In the next years, a major upcoming

challenge for DEGS-based WECs will be the migration of the technology from watt-scale up to the kilowatt-scale.^[141]

The concepts of DEGS-based WECs proposed to date exploit two different paradigms (Figure 18a), namely point power generation and distributed generation.^[140] Based on their dimensions compared with sea wavelengths (typically, on the order of 10^2 m), in wave energy literature,^[6] these paradigms are referred to as: 1) point absorbers (whose dimensions are much smaller than the wavelengths); and 2) attenuators (whose length is comparable with the wavelengths).

Up until now, point absorber DEGS-based WECs have been the most widely investigated.^[23,73,154,155] These systems generally rely on WEC layouts proposed in the past,^[6] from which they differ in that they hold a DEG PTO instead of conventional generators. Their operating principle is schematically shown in Figure 18a. The device includes a primary hydrodynamic interface, which interacts with the waves and serves as a kinetic and potential energy buffer, and a DEG PTO system, which is responsible for the mechanical-to-electrical power conversion. The primary interface either consists in a floating body (e.g., a heaving buoy^[23] or a pitching flap^[154]) or a volume of sea water canalized in a collector, called an oscillating water column (OWC).^[73] The interface is put into oscillation by the wave loads, and it drives the cyclical deformation of the DEG PTO. In addition to damping the system oscillations upon control, the DEG

participates in the WEC dynamics through its elastic response. Large elastomer volumes or high shear moduli of the DE can dramatically increase the WEC mechanical stiffness, hence limiting the achievable wave-induced deformations.

As a rule of thumb, point absorber WECs should be designed in such a way that their natural frequency matches the typical sea wave frequency. This condition, called resonance, is crucial to achieve efficient power capture from the waves.^[156] In DEG-based WECs, the natural frequency is the result of a balancing among inertial and hydrostatic loads (due to the primary interface) and DEG elastic loads.^[73,141]

The first point absorber DE-based WEC was proposed and demonstrated by Stanford Research Institute (USA) and Hyper Drive Corporation (Japan).^[50,148] In 2005, they built a small-scale demonstrator of a floating buoy WEC with DEG PTO and tested it at sea. The system, schematically represented in Figure 19a, included a tubular DEG (300 g DE acrylic material in total, 0.3 m diameter) connected through one edge to a floating barge, and through the other to a proof mass. The proof mass provided the DEG with axial prestretch, whereas the wave-induced relative motion between the barge and the mass provided cyclic stretching of the DEG. Tests in mild sea conditions led to an average power output of 0.25 W, with peaks of 1.2 W, though the authors claim that a power of 11 W could have been obtained with higher priming voltage.^[148] Other sea tests on similar or smaller prototypes were then carried out by some of the same authors,^[23,152] which managed to achieve cyclic energy densities over 100 mJ g^{-1} in dynamic operating conditions.^[23]

Recently, other theoretical studies and small laboratory demonstrators have been produced in which heaving buoy are combined with multilayer DE stacks^[155] or planar uniaxial DEGs.^[157] In addition to that, other point absorbing WECs have been proposed, which make use of different floater (e.g., a pitching flap) and DEG topology (e.g., diamond-shaped rotary DEG, as shown in Figure 19b).^[154]

WECs based on floating bodies include mechanical components and moving parts (e.g., floaters, hinges, etc.) whose complexity might compromise the WEC affordability, in spite of the advantageous features of the DEG. For this reason, in the past years, some research groups in the fields of DEs and WECs have focused their attention on DEGS-based OWCs.^[141] An OWC consists in a semisubmerged hollow collector partially filled by a volume of sea water. Wave-induced oscillations of the column generate alternate compressions/expansions of a pneumatic chamber, which delivers pneumatic energy to a PTO system (traditionally, a bidirectional air turbine).^[158] The DEGS-based OWC exploits the circular diaphragm DEG (Figure 2e) as the PTO system, as shown in Figure 19c, and it has no moving parts but the DEGs.

DEG-based OWCs have been systematically studied using consolidated approaches from the ocean engineering sector. First, dynamical models were set-up to describe the DEGS-OWC dynamics and assess its performance.^[47] Scaling rules for dynamically consistent testing of small-scale prototypes^[6] were formulated.^[48] Finally, small-scale prototypes were built and tested in wave tank basins, subject to artificial waves with scaled frequency and amplitude.^[48,73,141]

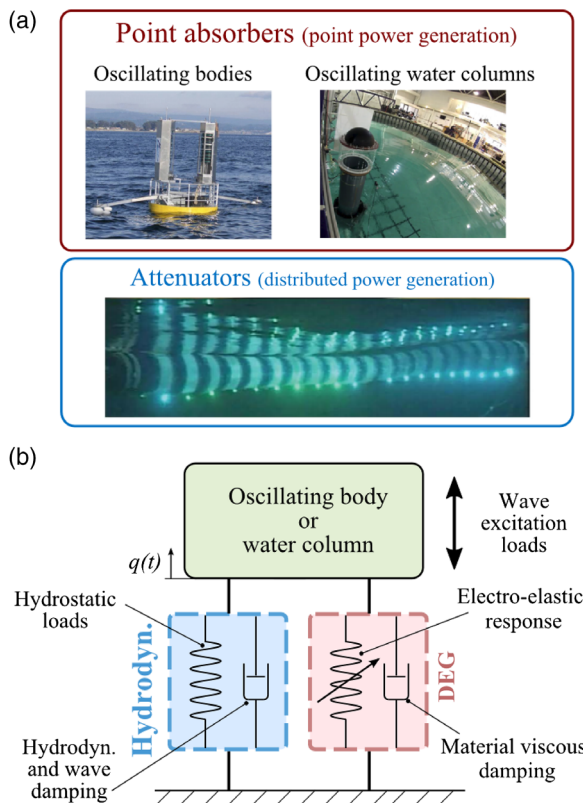


Figure 18. Overview on wave energy harvesting with DEGs. a) A classification of DEGS-based WECs proposed to date. b) Schematic of the general working principle of a point absorber WEC. Part (a) left: Reproduced with permission.^[23] Copyright 2012, Springer Nature. Part (a) bottom: Reproduced with permission.^[159] Copyright 2017, Elsevier.

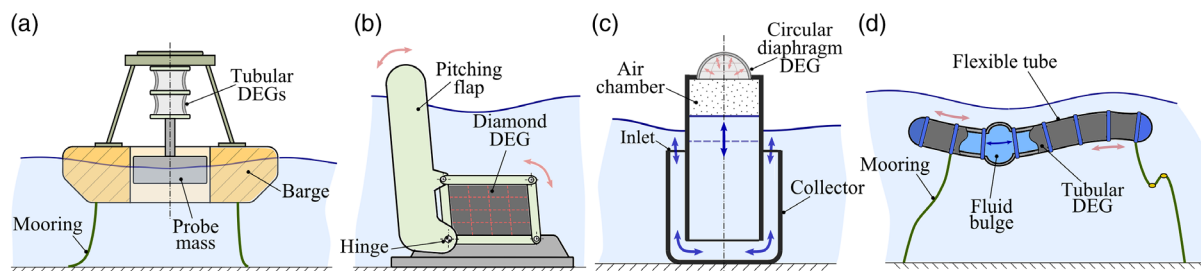


Figure 19. Some concepts of DEGS-based WECs. a) Impression of a heaving buoy WEC prototype with tubular DEG PTO, deployed by Chiba et al.^[148] b) Pitching flap with diamond DEG PTO, as proposed by Moretti et al.^[154] c) OWC with circular diaphragm DEG, as proposed by Vertechy et al.^[47] d) Bulge wave attenuator, investigated by Jean et al.^[49]

Two main wave tank campaigns were carried out on fully functional OWC prototypes subject to artificial waves at a scale of 1:40/1:30.^[48,73] VHB acrylic was selected as the DE material for these tests, as it allows simple manufacturing of decimeter-scale DEGs (DEGs with prestretched diameters up to 390 mm were deployed). The prototypes featured resonant behavior within the test wave frequency range. This was achieved by suitably designing the OWC collectors (e.g., L-shaped or U-shaped collectors, as shown in Figure 19c), so as to counterbalance the DEG's elastic stiffness with a large hydrodynamic inertia. In a first test,^[73] power outputs of up to 0.87 W (with 4.4 g of DE material) and wave-to-electrical conversion efficiencies of up to 18% were obtained. In a second test, power outputs of up to 3.8 W were obtained using larger DEG samples (with 19.5 g of DE material). Based on dynamic scaling rules, these powers are roughly equivalent to outputs on the order of 300–600 kW at full scale. In both tests, the DEGs were driven using an OT harvesting cycle (Section 3.1), they were subject to maximum electric fields on the order of 170 MV m⁻¹, and converted electrical energy densities of up to 140–190 mJ g⁻¹ per cycle.

Distributed attenuator WECs are envisaged to be completely free from mechanical parts (in contrast with floating point absorbers) or rigid structures (in contrast with OWCs), and to use the DE membranes both as the primary interface and the PTO. While these concepts aim at exploiting the DEGs' features (resilience, low weight, and low cost) at their best, they require remarkable research effort as they cannot build upon the operational experience of similar traditional WEC architectures.

A concept of DE-based attenuator has been proposed by SBM Offshore.^[49] The device, referred to as S3, consists in a tubular structure closed at both ends and filled with pressurized water (Figure 19d). The structure consists of a set of DEGs obtained by rolling electrode-coated DE membranes so as to form tubular segments. The segments are prestretched by water pressurization. The WEC length is comparable with typical wavelengths, therefore, different portions are subject to different hydrodynamic pressures, causing a bulge of fluid to propagate and generate local radial expansions of the different segments. The water bulge propagates within the tube as a standing wave. By tuning the natural frequencies of the structure modes, it is virtually possible to achieve large power capture efficiency in a wide range of sea states.

In 2010, a scaled model of S3 was tested in a wave tank. The prototype was 0.4 m in diameter and 11 m long (roughly, 1/36 the target full-scale length of 200 m), and it was made with silicone DE membranes with thin metal-film electrodes.^[49] During

the tests, radial strains in DE rings of up to 80% were recorded. The achieved peak electrical power was 2 W, although the authors claim that a significantly larger power output could have been obtained if larger electric fields (still much lower than the BD limit) were applied.

In addition to tank testing, numerical models of the fluid structure interaction of the S3 device with the waves were set up,^[159] dry-run generation tests on the DEG modules along with reliability tests were conducted,^[49] and layouts of scalable power electronics were identified (Section 3.3).^[125] As an important conclusion, the authors suggested that the peak electric field to be cyclically applied on the DE material should be significantly lower than the BD value (they suggest a value of 60 kV mm⁻¹ for silicones), for the system to reach a target lifetime on the order of 20 years (i.e., 45 × 10⁶ cycles at the typical wave frequencies). This would lead, in contrast, to convertible energy densities below 100 mJ g⁻¹ (roughly, 10 mW g⁻¹ at the waves); hence to heavier and bulkier designs.

The remarkable research effort conducted so far has demonstrated that DEGS-based WECs are a promising and potentially game-changing option for future WECs. However, some crucial challenges have yet to be addressed to make DEGs a viable option for wave energy. These include: 1) Development of robust sensing and control strategies (based on self-sensing or external DEG stretch sensing) and efficient power electronics (Section 3.3) capable to guarantee a WEC's functionality in highly variable random wave conditions. 2) Systematic investigation of cyclic DEG lifetime upon electromechanical loading, aimed at identifying threshold values for the maximum stretch and electric field compatible with a lifetime of 10⁶–10⁷ cycles.^[67] 3) Synthesis of new DE materials with optimized dielectric properties, i.e.: larger dielectric constant (which would provide large energy densities even at lower safe operating electric fields),^[160] or higher BD strength (which would provide wider safety margins if electric fields on the order of 100–200 kV mm⁻¹ are applied).^[77] 4) Upscaling of the technological processes for DE films manufacturing, compliant electrodes fabrication, and DEGs stacking and assembly.

5. Discussion and Conclusions

In this Review, a systematic analysis of the recent developments on DEGSs is proposed, considering different aspects related to electromechanics, materials, electronics, and sensing/control.

DEGSs are a promising technology for the conversion of mechanical energy into electrical energy with very large energy densities, good efficiency, and extreme low cost of the constituent materials. These features have made them an interesting option, and in the past decades, DEGSs have been studied for harvesting energy from different types of mechanical sources including ocean wave energy, human motion, and ambient vibrations. Several topologies have been investigated that feature different physical working principles including DEGS based on linear/rotary motions and inflatable structures. A number of different harvesting circuits and controllers have been analyzed ranging from low-cost/compact/milliwatt size devices for portable applications, up to high-performance/high-efficiency circuits for kilowatt-scale applications (e.g., energy harvesters from ocean waves or other renewable resources).

Despite their potential and the efforts done so far, DEGS have not yet seen their deployment as commercial products and they are still being studied in laboratories.

The development of DEGS as a viable conversion technology requires to face a number of challenges that lie ahead. Each of the different application fields of DEGSs calls for specific priorities.

For small-scale DEGS conceived for wearable/portable power systems, the relative high operating voltage in the range of kilovolts is a critical aspects for safety. Solutions should be devised to reduce voltages of at least one order of magnitude. To this end, high permittivity DE materials and processing solutions for the production of DE films with thickness of few micrometers are being studied. Voltage reduction would be also beneficial with respect to another big challenge for low-power DEGS, i.e., the study of effective/compact and low-cost solutions for the step-down electronics to provide a low-voltage usable output. Regarding this challenge, only few circuit topologies have been analyzed so far and further efforts could bring a large margin of improvement.

DEGS for large-scale/high-power systems such as those devised for renewable energy conversion have to face a number of challenges. While demonstrators developed so far have maximum dimensions of a few decimeters and power output of a few watts, significant technological effort is required to hit the target of meter-size kilowatt-scale DEGSs. This includes the upscaling of available manufacturing processes for thin-film DE membranes and multilayer dielectric-electrode DEGS assemblies, the identification of modular architectures which allow for an independent management/control/replacement of single portions of large DEGs, and the improvement of large-power bidirectional direct current electronics able to store the generated energy and/or deliver it to the electric grid. Moreover, for future large-scale DEGSs to be competitive with traditional technologies, the global efficiency should be improved. To this end, the synthesis of improved dielectric materials (especially silicones) is being studied, with the ambition of achieving improved dielectric properties, and reduced electromechanical losses. Implementation of large-scale DEGS-based energy harvesters requires large amounts of DE materials. To this end, research on biodegradable materials with low carbon footprint is key to cope with the environmental challenges that the energy market is now called to respond to.

In addition to that, the need for improved lifetime is a requirement that is common to most applications. Commercially, viable

DEGSs should be able to operate for several millions of cycles without performance degradation. Future developments on this topic require, first, the building of a reliable understanding of the degradation processes of DE under cyclical operation. On this topic, only few scientific results are available, with most of them focused on DE actuator applications only. The improvement of lifetime should then go through the study of new materials and apposite processing methods for dielectric layers, conductive electrodes, and their assembly.

The next future will be crucial to confirm the real potential of DEGSs. Thanks to the knowledge and operational experience gathered so far, the next few years might witness the spread of first milliwatt-scale commercial products. These might in turn trigger DEGS migration towards increasingly large and ambitious markets, finally hitting the target of large-scale renewable energy harvesting.

Appendix

A1. Energy Balance Equations for DEGs

By relying on an energy balance approach, we hereby present simple derivations of the equations for the local DEG response (Equation (2)), the global response of single-DoF DEGs (Equation (4)), and the maximum convertible energy (Equation (5)).

A2. Local Description

With reference to Figure 3, we indicate the side lengths (in the principal directions) of the unstretched membrane portion with l_{10} and l_{20} , and its initial thickness with t_0 . The real stress in a principal direction is the ratio of the nominal stress and the surface stretch ratio of the corresponding transversal cross section, namely: $\sigma_1 = s_1/(\lambda_2\lambda_3) = \lambda_1s_1$, and $\sigma_2 = s_2/(\lambda_1\lambda_3) = \lambda_2s_2$.

Following the approach proposed by Suo,^[53] it is possible to relate the material stresses to the stretches and the applied electric field via an electromechanical energy balance.

Assuming the electrode thickness negligible, the energy balance associated with an infinitesimal variation of the DEG patch configuration reads as follows

$$\begin{aligned} (s_1l_{20}t_0)\delta(l_{10}\lambda_1) + (s_2l_{10}t_0)\delta(l_{20}\lambda_2) + V\delta Q \\ = l_{10}l_{20}t_0\delta\Psi + l_{10}l_{20}t_0\delta\left(\frac{\epsilon}{2}E^2\right) \end{aligned} \quad (A1)$$

where the operator δ indicates an infinitesimal variation of a physical quantity; V and Q are the voltage difference between the electrodes and the residing charge, respectively. The first two terms on the left-hand side of Equation (A1) represent the mechanical work done by the applied stresses on the membrane (there is no stress in the thickness direction due to the plane-stress assumption); the third term is the energy supplied by the power electronics to the DE; the terms on the right-hand side are elastic and electrostatic potential energy variations, respectively. The equation can be rearranged by noticing that charge, voltage, and electric field are related as follows: $V = t_0\lambda_3E$ and $Q = \epsilon\lambda_1\lambda_2l_{10}l_{20}E$.

As the principal stretch variations $\delta\lambda_1$ and $\delta\lambda_2$ are independent (e.g., they can be zeroed separately), Equation (A1) leads to the Equation (2) in the article, which provides the principal stresses as a function of the stretches and the electric field.

Local formulations can be used to study complex DEG topologies. This can be achieved by combining the electromechanical constitutive Equation (2) with well-known equilibrium equations for continua^[55] and a set of boundary conditions.

A3. Global Description

If the deformation kinematics of a DEG is known, a straightforward computation of the equilibrium load as a function of the geometrical configuration and the applied voltage can be obtained through a global electromechanical energy balance, in the same fashion as Equation (A1).^[48] Neglecting electrical and mechanical losses, the global energy balance for a single-DoF DEG in correspondence of an infinitesimal state variation reads as follows

$$F_q \delta q + V \delta Q = \delta U_{el} + \delta U_{es}, \quad \text{with} \quad (A2)$$

$$U_{el} = \int_{\Omega} \Psi(\lambda_1, \lambda_2) d\Omega, \quad U_{es} = \frac{1}{2} C_{DEG} V^2$$

where U_{el} , the total elastic energy, is the integral of the strain-energy function over the DE volume; U_{es} is the total electrostatic energy; and C_{DEG} is the DEG capacitance. The terms on the left-hand side of Equation (A2) are the mechanical work and the electrical energy supplied to the DEG; those on the right-hand side represent the total variation in potential energy. Noting that, $C_{DEG} = Q/V$, Equation (A2) leads to Equation (4).

Based on energy balance in Equation (A2), the energy generated by the DEG during its state variation is the difference between the increase in the stored electrical energy and the energy supplied to the external circuit, namely

$$\delta U_{es} - V \delta Q = -\frac{V^2}{2} \delta C_{DEG} \quad (A3)$$

Energy is positively generated while the DEG capacitance decreases (i.e., $\delta C_{DEG} < 0$), hence motivating the control cycle shown in Figure 1, which only foresees a charge be present on the electrodes while the capacitance is decreasing.

A4. Maximum Convertible Energy

Based on the assumptions introduced in Section 2.4 (uniform stretches; constant BD field, E_{BD}), we compute the maximum convertible energy for a DEG using Equation (A3). Neglecting EMIs (i.e., (C') coincides with (D) in Figure 4a), the energy converted by the DEG reads as

$$W_e = - \oint \frac{V^2}{2} dC_{DEG} = \epsilon \Omega E_{BD}^2 \int_{(C)-(D)} \frac{dt}{t} = \epsilon \Omega E_{BD}^2 \log \frac{(\lambda_3)_{(D)}}{(\lambda_3)_{(C)}} \quad (A4)$$

where t is the stretched DE thickness, the first circulation integral is computed over loop (A)–(B)–(C)–(D)–(A) in Figure 4a, and the

capacitance is $C_{DEG} = \epsilon \Omega / t^2$. This equation immediately leads to Equation (5).

Acknowledgements

M.F. received funding from the Italian Ministry of Education, University and Research (MIUR) under the Program Department of Excellence, awarded to the Department of Industrial Engineering of the University of Trento.

Conflict of Interest

The authors declare no conflict of interest.

Keywords

dielectric elastomers, electro active polymers, energy harvesting

Received: June 8, 2020

Revised: July 19, 2020

Published online: August 23, 2020

- [1] P. D. Mitcheson, E. M. Yeatman, G. K. Rao, A. S. Holmes, T. C. Green, *Proc. IEEE* **2008**, *96*, 1457.
- [2] Y. K. Tan, S. K. Panda, in *Sustainable Wireless Sensor Networks*, IntechOpen, Rijeka, Croatia **2010**, pp. 15–43.
- [3] I. A. Anderson, I. A. Ieropoulos, T. McKay, B. O'Brien, C. Melhuish, *IEEE/ASME Trans. Mech.* **2010**, *16*, 107.
- [4] F. K. Shaikh, S. Zeadally, *Renewable Sustainable Energy Rev.* **2016**, *55*, 1041.
- [5] C. Wei, X. Jing, *Renewable Sustainable Energy Rev.* **2017**, *74*, 1.
- [6] A. Pecher, J. P. Kofoed, *Handbook of Ocean Wave Energy*, Springer, Berlin, Germany **2016**.
- [7] S. Watson, A. Moro, V. Reis, C. Baniotopoulos, S. Barth, G. Bartoli, F. Bauer, E. Boelman, D. Bosse, A. Cherubini, A. Croce, L. Fagiano, M. Fontana, A. Gambier, K. Gkoumas, C. Golightly, M. Latour, P. Jamieson, J. Kaldellis, A. Macdonald, J. Murphy, M. Muskulus, F. Petrini, L. Pigolotti, F. Rasmussen, P. Schild, R. Schmehl, N. Stavridou, J. Tande, N. Taylo, et al., *Renewable Sustainable Energy Rev.* **2019**, *113*, 109270.
- [8] A. Gallo, J. Simões-Moreira, H. Costa, M. Santos, *Renewable Sustainable Energy Rev.* **2016**, *65*, 800.
- [9] Renewables 2020, Global status report, Tech. rep., REN21 **2020**.
- [10] S. P. Beeby, T. Donnell, in *Energy Harvesting Technologies*, Springer, New York **2009**, pp. 129–161.
- [11] Z. L. Wang, *Faraday Discuss.* **2015**, *176*, 447.
- [12] C. R. Bowen, J. Taylor, E. LeBoulbar, D. Zabek, A. Chauhan, R. Vaish, *Energy Environ. Sci.* **2014**, *7*, 3836.
- [13] T.-H. Hsu, S. Manakasettharn, J. A. Taylor, T. Krupenkin, *Sci. Rep.* **2015**, *5*, 16537.
- [14] S. H. Kim, C. S. Haines, N. Li, K. J. Kim, T. J. Mun, C. Choi, J. Di, Y. J. Oh, J. P. Oviedo, J. Bykova, S. Fang, N. Jiang, Z. Liu, R. Wang, P. Kumar, R. Qiao, S. Priya, K. Cho, M. Kim, M. S. Lucas, L. F. Drummy, B. Maruyama, D. Y. Lee, X. Lepró, E. Gao, D. Albarq, R. Ovalle-Robles, S. J. Kim, R. H. Baughman, *Science* **2017**, *357*, 773.
- [15] S. Chiba, M. Waki, R. Kornbluh, R. Pelrine, *Smart Mater. Struct.* **2011**, *20*, 124006.
- [16] R. Pelrine, R. Kornbluh, Q. Pei, J. Joseph, *Science* **2000**, *287*, 836.

- [17] F. Carpi, I. Anderson, S. Bauer, G. Frediani, G. Gallone, M. Gei, C. Graaf, C. Jean-Mistra, W. Kaal, G. Kofod, M. Kollosche, R. Kornbluh, B. Lassen, M. Matysek, S. Michel, S. Nowak, B. O'Brien, Q. Pei, R. Pelrine, B. Rechenbach, S. Rosset, H. Shea, *Smart Mater. Struct.* **2015**, 24, 105025.
- [18] R. Kaltseis, C. Keplinger, S. J. A. Koh, R. Baumgartner, Y. F. Goh, W. H. Ng, A. Kogler, A. Tröls, C. C. Foo, Z. Suo, S. Bauer, *RSC Adv.* **2014**, 4, 27905.
- [19] S. Shian, J. Huang, S. Zhu, D. R. Clarke, *Adv. Mater.* **2014**, 26, 6617.
- [20] M. K. Senesky, *Ph.D. Thesis*, University of California, Berkeley **2015**.
- [21] M. Kiziroglou, E. Yeatman, in *Functional Materials for Sustainable Energy Applications*, Woodhead Publishing, London, UK **2012**, pp. 541–572.
- [22] H. Fu, E. M. Yeatman, *Energy Technol.* **2018**, 6, 2220.
- [23] R. D. Kornbluh, R. Pelrine, H. Prahlad, A. Wong-Foy, B. McCoy, S. Kim, J. Eckerle, T. Low, in *Electroactivity in Polymeric Materials*, Springer, Boston, MA **2012**, pp. 67–93.
- [24] R. Pelrine, R. D. Kornbluh, J. Eckerle, P. Jeuck, S. Oh, Q. Pei, S. Stanford in *8th Annual International Symposium on Smart Structures and Materials*, SPIE–The Int. Society for Optical Engineering, Newport Beach, CA **2001**, pp. 148–156.
- [25] A. York, J. Dunn, S. Seelecke, *Smart Mater. Struct.* **2013**, 22, 094015.
- [26] T. G. McKay, S. Rosset, I. A. Anderson, H. Shea, *Smart Mater. Struct.* **2015**, 24, 015014.
- [27] A. O. Halloran, *J. Appl. Phys.* **2008**, 104, 9.
- [28] J. C. Simo, R. L. Taylor, *Comput. Methods Appl. Mech. Eng.* **1991**, 85, 273.
- [29] G. Holzapfel, *Nonlinear Solid Mechanics. A Continuum Approach for Engineering*, Wiley, Chichester, UK **2000**.
- [30] P. Steinmann, M. Hossain, G. Possart, *Arch. Appl. Mech.* **2012**, 82, 1183.
- [31] S. J. A. Koh, C. Keplinger, T. Li, S. Bauer, Z. Suo, *IEEE/ASME Trans. Mech.* **2011**, 16, 33.
- [32] S. J. A. Koh, X. Zhao, Z. Suo, *Appl. Phys. Lett.* **2009**, 94, 262902.
- [33] J. Huang, S. Shian, Z. Suo, D. R. Clarke, *Adv. Funct. Mater.* **2013**, 23, 5056.
- [34] I. A. Anderson, S. Rosset, T. McKay, H. Shea, *Opt. Photonics*, **2014**, 9056, 90560Q.
- [35] Z.-Q. Song, K. Ohyama, S. Shian, D. R. Clarke, S. Zhu, *Smart Mater. Struct.* **2019**, 29, 015018.
- [36] L. Dorfmann, R. W. Ogden, *Nonlinear Theory of Electroelastic and Magnetoelastic Interactions*, Springer, New York **2014**.
- [37] W. Yin, Z. Jin-Xiong, W. Xiao-Hong, L. Bo, Z. Ling, *Chin. Phys. Lett.* **2013**, 30, 066103.
- [38] G. Moretti, M. Fontana, R. Vertechy, in *ASME 2013 Conf. on Smart Materials, Adaptive Structures and Intelligent Systems*, American Society of Mechanical Engineers, Snowbird, UT **2013**, p. V001T03A039.
- [39] G. Moretti, M. Fontana, R. Vertechy, *J. Intell. Mater. Syst. Struct.* **2015**, 26, 740.
- [40] Y. Zhu, H. Wang, D. Zhao, J. Zhao, *Smart Mater. Struct.* **2011**, 20, 115022.
- [41] E. Bortot, M. Gei, *Extreme Mech. Lett.* **2015**, 5, 62.
- [42] Y. Jiang, S. Liu, M. Zhong, L. Zhang, N. Ning, M. Tian, *Nano Energy* **2020**, 71, 104606.
- [43] G. Berselli, R. Vertechy, G. Vassura, V. Parenti-Castelli, *IEEE/ASME Trans. Mech.* **2011**, 16, 67.
- [44] M. Hodgins, A. York, S. Seelecke, *Smart Mater. Struct.* **2013**, 22, 094016.
- [45] H. Wang, Y. Zhu, L. Wang, J. Zhao, *J. Intell. Mater. Syst. Struct.* **2012**, 23, 885.
- [46] R. Kaltseis, C. Keplinger, R. Baumgartner, M. Kaltenbrunner, T. Li, P. Mächler, R. Schwödiauer, Z. Suo, S. Bauer, *Appl. Phys. Lett.* **2011**, 99, 162904.
- [47] R. Vertechy, G. P. P. Rosati, M. Fontana, *J. Vib. Acoustics* **2015**, 137, 011016.
- [48] G. Moretti, G. P. R. Papini, L. Daniele, D. Forehand, D. Ingram, R. Vertechy, M. Fontana, *Proc. R. Soc. A* **2019**, 475, 20180566.
- [49] P. Jean, A. Wattez, G. Ardoise, C. Melis, R. Van Kessel, A. Fourmon, E. Barrabino, J. Heemskerck, J. P. Queau, in *Proc. of SPIE Smart Structures and Materials + Nondestructive Evaluation and Health Monitoring*, Vol. 8340, SPIE–The Int. Society for Optical Engineering, San Diego, CA **2012**, p. 83400C.
- [50] R. D. Kornbluh, J. Eckerle, B. McCoy, *SPIE Newsroom* **2011**, <https://doi.org/10.1117/2.1201106.003749>.
- [51] D. Yurchenko, Z. Lai, G. Thomson, D. V. Val, R. V. Bobryk, *Appl. Energy* **2017**, 208, 456.
- [52] X. Zhao, W. Hong, Z. Suo, *Phys. Rev. B* **2007**, 76, 134113.
- [53] Z. Suo, *Acta Mech. Solida Sin.* **2010**, 23, 549.
- [54] M. Mehnert, M. Hossain, P. Steinmann, *Int. J. Non-Linear Mech.* **2018**, 106, 13.
- [55] G. A. Holzapfel, *Nonlinear Solid Mechanics – A Continuum Approach for Engineering*, vol. 24, Wiley, Chichester **2000**.
- [56] C. C. Foo, S. Cai, S. J. A. Koh, S. Bauer, Z. Suo, *J. Appl. Phys.* **2012**, 111, 034102.
- [57] E. Bortot, R. Denzer, A. Menzel, M. Gei, *Int. J. Solids Struct.* **2016**, 78, 205.
- [58] G. Rizzello, D. Naso, S. Seelecke, *IFAC-PapersOnLine* **2017**, 50, 4855.
- [59] L. A. Mihai, A. Goriely, *Proc. R. Soc. A: Math. Phys. Eng. Sci.* **2017**, 473, 20170607.
- [60] F. B. Madsen, A. E. Daugaard, S. Hvilsted, A. L. Skov, *Macromol. Rapid Commun.* **2016**, 37, 378.
- [61] Y. Chen, L. Agostini, G. Moretti, M. Fontana, R. Vertechy, *Smart Mater. Struct.* **2019**, 28, 114001.
- [62] A. Dorfmann, R. Ogden, *Int. J. Solids Struct.* **2003**, 40, 2699.
- [63] E. Garnell, C. Rouby, O. Doaré, *J. Sound Vib.* **2019**, 459, 114836.
- [64] T. McKay, B. O'Brien, E. Calius, I. Anderson, *Smart Mater. Struct.* **2010**, 19, 055025.
- [65] G. Moretti, M. Righi, R. Vertechy, M. Fontana, *Polymers* **2017**, 9, 283.
- [66] Y. J. Lee, P. Caspari, D. M. Opris, F. A. Nuesch, S. Ham, J.-H. Kim, S.-R. Kim, B.-K. Ju, W. K. Choi, *J. Mater. Chem. C* **2019**, 7, 3535.
- [67] C. Jean-Mistral, G. Jacquet-Richardet, A. Sylvestre, *Polym. Test.* **2020**, 81, 106198.
- [68] S. Rosset, O. A. Araromi, S. Schlatter, H. R. Shea, *J. Visualized Exp.* **2016**, 108, e53423.
- [69] B. Fasolt, M. Hodgins, G. Rizzello, S. Seelecke, *Sens. Actuators A: Phys.* **2017**, 265, 10.
- [70] Elastosil Films Catalogue, Wacker, <https://www.wacker.com/h/en-us/silicone-rubber/silicone-films/elastosil-film-2030/p/000038005> (accessed: August 2020).
- [71] F. Förster-Zügel, S. Solano-Arana, F. Klug, H. F. Schlaak, *Smart Mater. Struct.* **2019**, 28, 075042.
- [72] D. Gatti, H. Haus, M. Matysek, B. Frohnappel, C. Tropea, H. F. Schlaak, *Appl. Phys. Lett.* **2014**, 104, 052905.
- [73] G. Moretti, E. C. N. Silva, J. N. Reddy, *Smart Mater. Struct.* **2018**, 27, 035015.
- [74] W. Jawjit, C. Kroeze, S. Rattanapan, *J. Cleaner Prod.* **2010**, 18, 403.
- [75] A. A. Shah, F. Hasan, Z. Shah, N. Kanwal, S. Zeb, *Int. Biodeterior. Biodegrad.* **2013**, 83, 145.
- [76] F. Carpi, D. D. Rossi, *IEEE Trans. Dielectr. Electr. Insul.* **2005**, 12, 835.
- [77] L. Yu, A. L. Skov, *RSC Adv.* **2017**, 7, 45784.
- [78] F. Madsen, L. Yu, P. Mazurek, A. Skov, *Smart Mater. Struct.* **2016**, 25, 075018.
- [79] S. Risse, B. Kussmaul, H. Krüger, G. Kofod, *RSC Adv.* **2012**, 2, 9029.
- [80] T. Vu-Cong, C. Jean-Mistral, A. Sylvestre, *Smart Mater. Struct.* **2013**, 22, 025012.

- [81] H.-Y. Ong, M. Shrestha, G.-K. Lau, *Appl. Phys. Lett.* **2015**, *107*, 132902.
- [82] T. A. Kim, H. S. Kim, S. S. Lee, M. Park, *Carbon* **2012**, *50*, 444.
- [83] D. McCoul, S. Rosset, S. Schlatter, H. Shea, *Smart Mater. Struct.* **2017**, *26*, 125022.
- [84] M. Matysek, P. Lotz, H. Schlaak, *IEEE Trans. Dielectr. Electr. Insul.* **2011**, *18*, 89.
- [85] C. de Saint-Aubin, S. Rosset, S. Schlatter, H. Shea, *Smart Mater. Struct.* **2018**, *27*, 074002.
- [86] M. Hill, G. Rizzello, S. Seelecke, in *Proc. of SPIE – The International Society for Optical Engineering* **2017**, Vol. 10163, p. 101630X.
- [87] Y. Chen, L. Agostini, M. Fontana, G. Moretti, R. Vertechy, in *ASME 2018 Conf. on Smart Materials, Adaptive Structures and Intelligent Systems*, American Society of Mechanical Engineers Digital Collection **2018**, p. V001T03A028.
- [88] Y. Chen, Y. Chen, L. Agostini, G. Moretti, G. Berselli, M. Fontana, R. Vertechy, in *Proc. of SPIE Smart Structures + Nondestructive Evaluation*, Vol. 10966, SPIE–The Int. Society for Optical Engineering, Denver, CO **2019**, p. 1096616.
- [89] A. Iannarelli, M. G. Niasar, in *Proc. of SPIE Smart Structures and Materials + Nondestructive Evaluation and Health Monitoring*, Vol. 10163, SPIE–The Int. Society for Optical Engineering, Portland, OR **2017**, p. 1016326.
- [90] S. Cadwell, R. Merrill, C. Sloman, F. Yost, *Ind. Eng. Chemistry Analytical Edition* **1940**, *12*, 19.
- [91] W. Mars, A. Fatemi, *Rubber Chem. Technol.* **2004**, *77*, 391.
- [92] P.-Y. Le Gac, M. Arhant, P. Davies, A. Muhr, *Mater. Design* **2015**, *65*, 462.
- [93] W. Fan, Y. Wang, S. Cai, *Polym. Test.* **2017**, *61*, 373.
- [94] T. Li, S. Qu, W. Yang, *J. Appl. Phys.* **2012**, *112*, 034119.
- [95] C. Graf, J. Maas, D. Schapeler, *Proc. of SPIE Smart Structures and Materials + Nondestructive Evaluation and Health Monitoring*, (Ed: Y. Bar-Cohen), Vol. 7642, SPIE–The Int. Society for Optical Engineering, San Diego, CA **2010**, p. 764217.
- [96] P. Fan, H. Chen, B. Li, Y. Wang, *Eur. Lett.* **2017**, *120*, 47007.
- [97] P. Fan, H. Chen, *Polymers* **2018**, *10*, 1341.
- [98] T. A. Gisby, B. M. O'Brien, I. A. Anderson, *Appl. Phys. Lett.* **2013**, *102*, 193703.
- [99] P. Zanini, G. Rizzello, S. Seelecke, J. Rossiter, M. Homer, in *Proc. of SPIE Smart Structures and Materials + Nondestructive Evaluation and Health Monitoring*, Vol. 10594, SPIE–The Int. Society for Optical Engineering, Denver, CO **2018**, p. 105941J.
- [100] Y. Wang, L. Zhu, G. Zhang, L. Zhong, H. Chen, *AIP Adv.* **2018**, *8*, 085310.
- [101] J.-B. Cao, M. Lan, E. Shi-Ju, Z. Gao, H.-P. Luo, X.-M. Li, X. Pan, *AIP Adv.* **2019**, *9*, 115112.
- [102] P. Illenberger, K. Takagi, H. Kojima, U. K. Madawala, I. A. Anderson, *IEEE Trans. Power Electron.* **2016**, *32*, 6904.
- [103] P. Zanini, J. Rossiter, M. Homer, *Smart Mater. Struct.* **2017**, *26*, 035037.
- [104] T. McKay, B. O'Brien, E. Calius, I. Anderson, *Appl. Phys. Lett.* **2010**, *97*, 062911.
- [105] P. Illenberger, S. Rosset, U. Madawala, I. Anderson, *IEEE Trans. Ind. Electron.* **2020**, <https://doi.org/10.1109/tie.2020.3003591>.
- [106] Y. Wang, L. Zhu, G. Zhang, H. Chen, *Appl. Phys. Lett.* **2018**, *113*, 113904.
- [107] T. G. McKay, B. M. O'Brien, E. P. Calius, I. A. Anderson, *Appl. Phys. Lett.* **2011**, *98*, 142903.
- [108] C. Jean-Mistral, T. V. Cong, A. Sylvestre, *Appl. Phys. Lett.* **2012**, *101*, 162901.
- [109] C. Jean-Mistral, T. Vu-Cong, A. Sylvestre, *Smart Mater. Struct.* **2013**, *22*, 104017.
- [110] C. Lagomarsini, C. Jean-Mistral, S. Monfray, A. Sylvestre, *Smart Mater. Struct.* **2019**, *28*, 104003.
- [111] P. K. Illenberger, P. Zanini, S. Rosset, U. K. Madawala, I. A. Anderson, in *Proc. of SPIE – The International Society for Optical Engineering* **2018**, Vol. 10594, p. 1059429.
- [112] C. Lagomarsini, C. Jean-Mistral, G. Lombardi, A. Sylvestre, *Smart Mater. Struct.* **2019**, *28*, 035003.
- [113] A. T. Mathew, C. Liu, T. Y. N. Ng, S. J. A. Koh, *Sens. Actuators A: Phys.* **2019**, *294*, 61.
- [114] A. T. Mathew, V. T. V. Khanh, M. D. B. M. Aliffi, C. Liu, S. J. A. Koh, *J. Intell. Mater. Syst. Struct.* **2020**, *31*, 152.
- [115] H. S. Kim, J.-H. Kim, J. Kim, *Int. J. Prec. Eng. Manuf.* **2011**, *12*, 1129.
- [116] J. Due, S. Munk-Nielsen, R. Nielsen, *5th IET Int. Conf. on Power Electronics, Machines and Drives*, Institution of Engineering and Technology, **2010**.
- [117] L. Eitzen, T. Hoffstadt, J. Maas, in *Proc. of SPIE Smart Structures and Materials + Nondestructive Evaluation and Health Monitoring*, Vol. 8687, SPIE–The Int. Society for Optical Engineering, San Diego, CA **2013**, p. 86870D.
- [118] L. Eitzen, C. Graf, J. Maas, in *Proc. of SPIE Smart Structures and Materials + Nondestructive Evaluation and Health Monitoring*, Vol. 8687, SPIE–The Int. Society for Optical Engineering, San Diego, CA **2013**, p. 86870P.
- [119] R. Panigrahi, S. K. Mishra, A. K. Srivastava, S. Basu, *IEEE Trans. Ind. Electron.* **2019**, *66*, 3507.
- [120] H. C. Lo, Converters for Milliwatt Dielectric Elastomer Generators, Ph.D. Thesis, University of Auckland **2015**.
- [121] I. A. Anderson, B. M. O'Brien, T. A. Gisby, T. G. McKay, H. C. Lo, US patent US20140247624A1 **2011**.
- [122] T. Ikegame, K. Takagi, in *Proc. of SPIE Smart Structures and Materials + Nondestructive Evaluation and Health Monitoring*, Vol. 10163, SPIE–The Int. Society for Optical Engineering, Denver, CO **2018**, p. 1016331.
- [123] T. Ikegame, K. Takagi, T. Ito, H. Kojima, H. Yoshikawa, in *Proc. of SPIE Smart Structures and Materials + Nondestructive Evaluation and Health Monitoring*, Vol. 10163, SPIE–The Int. Society for Optical Engineering, Portland, OR **2017**, p. 1016331.
- [124] L. Eitzen, C. Graf, J. Maas, *IECON 2011-37th Annual Conference on IEEE Industrial Electronics Society*, IEEE, Melbourne, Victoria, AU **2011**, pp. 1226–1231.
- [125] T. Todorovic, R. van Kessel, P. Bauer, J. A. Ferreira, *IEEE J. Emerging Sel. Top. Power Electron.* **2015**, *3*, 1171.
- [126] T. Todorovic, P. Bauer, J. A. Ferreira, R. van Kessel, *IEEE Energy Conversion Congress and Exposition*, IEEE, Denver, CO **2013**.
- [127] C. Graf, L. Eitzen, J. Maas, in *Proc. of the 2011 14th European Conference on Power Electronics and Applications*, IEEE, Birmingham, UK **2011**, pp. 1–10.
- [128] R. van Kessel, B. Czech, P. Bauer, J. A. Ferreira, in *IECON 2010 – 36th Annual Conf. on IEEE Industrial Electronics Society*, IEEE **2010**.
- [129] S. Priya, H.-C. Song, Y. Zhou, R. Varghese, A. Chopra, S.-G. Kim, I. Kanno, L. Wu, D. S. Ha, J. Ryu, R. G. Polcawich, *Energy Harvest. Syst.* **2019**, *4*, 3.
- [130] H. Liu, J. Zhong, C. Lee, S.-W. Lee, L. Lin, *Appl. Phys. Rev.* **2018**, *5*, 041306.
- [131] M. Lallart, P.-J. Cottinet, D. Guyomar, L. Lebrun, *J. Polym. Sci. B: Polym. Phys.* **2012**, *50*, 523.
- [132] C. Jean-Mistral, S. Basrour, J. Chaillout, *Smart Mater. Struct.* **2010**, *19*, 105006.
- [133] T. R. Ray, J. Choi, A. J. Bandodkar, S. Krishnan, P. Gutruf, L. Tian, R. Ghaffari, J. A. Rogers, *Chem. Rev.* **2019**, *119*, 5461.
- [134] R. Riemer, A. Shapiro, *J. NeuroEng. Rehabil.* **2011**, *8*, 22.
- [135] R. D. Kornbluh, R. Pelrine, Q. Pei, R. Heydt, S. Stanford, S. Oh, J. Eckerle, in *Proc. of SPIE – The International Society for Optical Engineering*, Vol. 4698 **2002**, pp. 254–270.

- [136] N. Savage, IEEE Spectrum, <http://spectrum.ieee.org/green-tech/fuel-cells/squishy-power-generators> (accessed: August 2020).
- [137] H. Lai, K. Reid, *J. Rehabil. Assistive Technol. Eng.* **6**, 2019.
- [138] C. Jean-Mistral, S. Basrour, J.-J. Chaillout, in *Proc. of SPIE Smart Structures and Materials + Nondestructive Evaluation and Health Monitoring*, Vol. 6927, SPIE—The Int. Society for Optical Engineering, San Diego, CA **2008**, p. 692716.
- [139] C. Jean-Mistral, S. Basrour, *Opt. Photonics* **2010**, 7642, 764209.
- [140] S. Chiba, M. Waki, *Sustainable Chem. Pharm.* **2020**, 15, 100205.
- [141] G. Moretti, G. Moretti, M. S. Herran, D. Forehand, M. Alves, H. Jeffrey, R. Vertechy, M. Fontana, *Renewable Sustainable Energy Rev* **2020**, 117, 109430.
- [142] H.-M. Kim, *J. Ocean Eng. Mar. Energy* **2018**, 4, 343.
- [143] G. Thomson, Z. Lai, D. V. Val, D. Yurchenko, *J. Sound Vib.* **2019**, 442, 167.
- [144] G. Moretti, G. Malara, A. Scialò, L. Daniele, A. Romolo, R. Vertechy, M. Fontana, F. Arena, *Renewable Energy* **2020**, 146, 628.
- [145] S. P. Beeby, M. J. Tudor, N. White, *Meas. Sci. Technol.* **2006**, 17, R175.
- [146] P. Fan, L. Zhu, H. Chen, B. Luo, *Smart Mater. Struct.* **2018**, 27, 115023.
- [147] N. D. Laws, B. P. Epps, *Renewable Sustainable Energy Rev.* **2016**, 57, 1245.
- [148] S. Chiba, M. Waki, K. Masuda, T. Ikoma, in *OCEANS 2010 IEEE-Sydney*, IEEE, Sydney, AU **2010**, pp. 1–5.
- [149] J. Maas, C. Graf, *Smart Mater. Struct.* **2012**, 21, 064006.
- [150] S. Chiba, K. Hasegawa, M. Waki, K. Fujita, K. Ohyama, S. Zhu, *J. Mater. Sci. Eng. A* **2017**, 7, 121.
- [151] Z. Lai, J. Wang, C. Zhang, G. Zhang, D. Yurchenko, *Energy Convers. Manage.* **2019**, 199, 111993.
- [152] S. Chiba, M. Waki, K. Fujita, K. Masuda, T. Ikoma, *J. Mater. Sci. Eng. B* **2017**, 7, 1.
- [153] K. Ruehl, D. Bull, *Oceans*, IEEE, Hampton Roads, VA **2012**.
- [154] G. Moretti, M. Fontana, R. Vertechy, *Meccanica* **2015**, 50, 2797.
- [155] X. Lv, L. Liu, Y. Liu, J. Leng, *Smart Mater. Struct.* **2015**, 24, 115036.
- [156] J. Falnes, *Ocean Waves and Oscillating Systems: Linear Interactions Including Wave-Energy Extraction*, Cambridge University Press, Cambridge **2002**.
- [157] P. C. Binh, K. K. Ahn, *Int. J. Precis. Eng. Manuf.* **2016**, 17, 1175.
- [158] A. F. Falcão, J. C. Henriques, *Renewable Energy* **2016**, 85, 1391.
- [159] A. Babarit, J. Singh, C. Mélis, A. Watez, P. Jean, *J. Fluids Struct.* **2017**, 74, 356.
- [160] S. J. Dünki, E. Cuervo-Reyes, D. M. Opris, *Polym. Chem.* **2017**, 8, 715.



Giacomo Moretti is a postdoctoral researcher at Scuola Sant'Anna (Pisa, Italy). He received the M.S. (2013) in energy engineering from the University of Pisa and the Ph.D. (2017) from Scuola Sant'Anna. He was: honors student at Scuola Sant'Anna (2008–2013); visiting student at the Fermi National Accelerator Laboratory (USA); visiting Ph.D. student at the University of Edinburgh (UK); and visiting researcher at the University of Trento (Italy). His research focuses on modeling and characterization of multifunctional transducers, with a special focus on energy-harvesting applications.



Samuel Rosset received the M.Sc. and Ph.D. degrees in microengineering from the EPFL, Switzerland, in 2004 and 2009, respectively. He is a senior research fellow at the Auckland Bioengineering Institute at the University of Auckland, New Zealand. He has been working on soft transducers since 2005, with a focus on optical and biomedical applications, as well as on the fabrication processes of these devices.



Rocco Vertechy is an associate professor at the Industrial Engineering Department of the University of Bologna. He received his M.Sc. in mechanical engineer degree in 2001 and Ph.D. degree in mechanics of machines in 2005. He was a research assistant at the University of Canterbury (New Zealand), visiting researcher at Stanford University (California); assistant professor at the Scuola Superiore Sant'Anna (Italy). He has been scientific responsible in a number of funded research projects related to the application of DE transducers for machine actuation and energy harvesting.



Iain A. Anderson is a professor with the Auckland Bioengineering Institute (ABI) and the Department of Engineering Science at the University of Auckland. He has worked as a product designer (Fisher and Paykel Ltd.) and a research engineer (Industrial Research Ltd., New Zealand). In 2006, he founded the Biomimetics Laboratory (<https://www.auckland.ac.nz/en/abi/our-research/research-groups-themes/biomimetics-laboratory.html>) at the ABI. His research interests include control and self-sensing aspects of artificial muscle technology for energy harvesting and soft robotics applications.



Marco Fontana is an associate professor in mechanical engineering at the University of Trento. He received the M.Sc. in mechanical engineering from University of Pisa in 2003 and his Ph.D. in robotics from Scuola Superiore Sant'Anna, in 2008. His research interests include the design and control of robotic systems such as wearable exoskeletons, haptics, soft actuators and energy harvesters. Since 2010, he has been the PI of different projects related with the development of new electromechanical technologies for robotics and renewable energy harvesting.